Thermodynamics of Hamiltonian anyons with applications to quantum heat engines

Joe Dunlop,^{1,*} Álvaro Tejero,^{2,3,†} Michalis Skotiniotis,^{2,3,‡} and Daniel Manzano^{2,3,§}

¹Physics and Astronomy, University of Exeter, Exeter EX4 4QL, United Kingdom
²Electromagnetism and Condensed Matter Department, Universidad de Granada, 18071 Granada, Spain
³Instituto Carlos I de Física Teórica y Computacional, Universidad de Granada, 18071 Granada, Spain
(Dated: February 27, 2025)

The behavior of a collection of identical particles is intimately linked to the symmetries of their wavefunction under particle exchange. Topological anyons, arising as quasiparticles in low-dimensional systems, interpolate between bosons and fermions, picking up a complex phase when exchanged. Recent research has demonstrated that similar statistical behavior can arise with mixtures of bosonic and fermionic pairs, offering theoretical and experimental simplicity. We introduce an alternative implementation of such *statistical anyons*, based on promoting or suppressing the population of symmetric states via a symmetry generating Hamiltonian. The scheme has numerous advantages: anyonic statistics emerge in a single particle pair, extending straightforwardly to larger systems; the statistical properties can be dynamically adjusted; and the setup can be simulated efficiently. We show how exchange symmetry can be exploited to improve the performance of heat engines, and demonstrate a reversible work extraction cycle in which bosonization and fermionization replace compression and expansion strokes. Additionally, we investigate emergent thermal properties, including critical phenomena, in large statistical anyon systems.

I. INTRODUCTION

Symmetry under particle exchange is an essential property of quantum systems [1–3]. The indistinguishability of quantum particles means that swapping them results in no measurable difference. Exchanging a pair of identical particles in states $|\psi_1\rangle$ and $|\psi_2\rangle$ can therefore only change the joint state by a global phase:

$$|\psi_2, \psi_1\rangle = e^{i\pi\varphi} |\psi_1, \psi_2\rangle, \qquad (1)$$

where $\varphi = 2n$ for bosons and $\varphi = 2n+1$ for fermions, with $n \in \mathbb{N}_0$. In three dimensions these are the only two possibilities due to the spin-statistics theorem [4]. However, quasiparticles in two dimensional systems can acquire an arbitrary phase. These particles, which do not conform to either fermionic or bosonic behavior, are known as anyons [5, 6] and play a pivotal role in the quantum Hall effect [7, 8] as well as universal topological quantum computing [9, 10]. Experimental evidence for anyons has been observed via Aharonov-Bohm interference [11] and anyonic collisions [12]. Recently, anyons have also been simulated on a trapped-ion processor [13].

Exchange symmetry is deeply linked to the thermodynamic properties of identical particle systems. The antisymmetry of fermions implies that no two can share exactly the same state (the Pauli exclusion principle) leading to a repulsive exchange interaction; whereas bosons can cluster without restriction. This distinction underlies the difference between Fermi-Dirac and Bose-Einstein statistics [14–18]. Anyon systems, in contrast, exhibit

fractional statistics which can be modeled by a generalized exclusion principle [19] allowing their thermal properties to interpolate between those of fermions and bosons [20, 21].

The physical implementation of anyons is challenging. In Ref. [22], Myers and Deffner establish an alternative approach. Instead of analyzing the behavior of real low-dimensional topological anyons, the authors consider an ensemble composed of pairs of particles with either bosonic or fermionic symmetry introducing the concept of statistical anyons. This model is found to be equivalent to generalized exclusion statistics, which closely approximates the thermodynamic properties of topological anyons. In this paper, we present a novel approach to statistical anyons illustrated in Fig. 1. Rather than working with an ensemble of bosonic and fermionic systems, we instead consider a *single* multi-particle system in a mixed quantum state—which overlaps with both symmetric and antisymmetric subspaces—with the intrinsic symmetry of the particles encoded into a latent degree of freedom. For a carefully engineered Hamiltonian the thermal equilibrium state interpolates between fermionic and bosonic symmetries. We refer to this new construction as Hamiltonian anyons.

Hamiltonian anyons possess a number of intriguing properties. In particular, the balance between fermionic and bosonic statistics can be tuned, or even dynamically altered, via externally controlled Hamiltonian parameters or by changing the temperature. We find that, for larger systems, the crossover between bosonic and fermionic regimes results in first and second-order phase transitions which can be exploited for the construction of quantum heat engines.

Aside from their transformative technological applications, the study of heat engines has been pivotal in the conceptual development of thermodynamics, a tradition which continues in the modern field of quantum

^{*} j.dunlop@exeter.ac.uk

[†] atejero@onsager.ugr.es

[†] mskotiniotis@onsager.ugr.es

[§] manzano@onsager.ugr.es

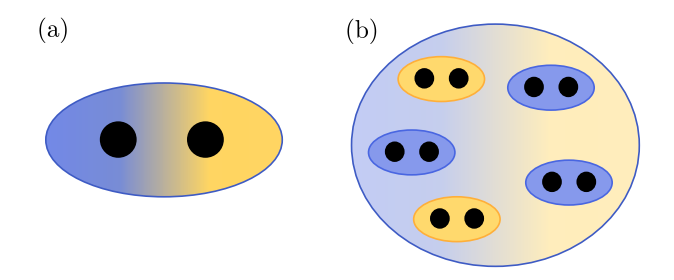


FIG. 1. An illustration of two statistical approaches to anyons. Orange represents fermionic exchange symmetry, while blue indicates bosonic. (a) Hamiltonian anyons as introduced in this paper. A single pair of particles occupies a mixed quantum state which overlaps with both the symmetric and antisymmetric subspaces. The framework can easily be extended to N>2 particles. (b) Statistical anyons, introduced in [22] as an ensemble of particle pairs, each in a purely symmetric or antisymmetric state. Collectively, the statistical properties of the ensemble interpolate between those of bosons and fermions.

thermodynamics [23–27]. Since the pioneering contributions of Alicki [28], Linden [29] and Scully [30], many different models of quantum engine have been proposed, extending and refining the concepts of heat and work [28, 31]. This research also brings to light the thermodynamic role of uniquely quantum resources such as coherence and squeezing [32, 33]. The effect of particle symmetry on heat engines has recently been addressed, with bosons typically outperforming fermions and distinguishable particles as a working medium [34]. Furthermore, a work extraction cycle relying on fermionization and bosonization, rather than conventional heating and cooling, has been experimentally demonstrated using Feshbach resonance [35].

We put forth two heat engines using Hamiltonian anyons. In the first, a Stirling cycle, the system is actively driven between fermionic and bosonic statistics, achieving Carnot efficiency in the limit of quasistatic and isothermal driving. In the second, an Otto cycle, we rapidly vary the frequency of the confining potential, with the system transitioning passively between fermionic and bosonic regimes during heating and cooling. We find that both the efficiency and power of the cycle is substantially enhanced as compared to a purely fermionic or bosonic medium.

The paper is organized as follows. Section II introduces the requisite mathematical background for the treatment of exchange symmetry in quantum mechanical systems. Section III introduces a model Hamiltonian and analyzes the equilibrium thermal properties of a multi-particle system before characterizing the fermion-boson phase transition. Based on this, two heat engines are proposed in Section IV. In Section V we consider the simulation of Hamiltonian anyons in digital quantum computers. We summarize and conclude in Section VI.

II. HILBERT SPACES UNDER EXCHANGE SYMMETRY

This section explores the central idea behind the construction of multi-particle systems with varying statistical properties. The approach utilizes auxiliary degrees of freedom for each particle to control their collective statistical behavior under particle exchange. To keep the focus on conceptual understanding, we offer an expository description here, with the comprehensive mathematical treatment provided in Appendix A.

To illustrate the construction, consider a pair of confined particles, each with two degrees of freedom. For later clarity, we assume one degree of freedom relates to the energy of the particles, while the other corresponds to their spin. The state space for each particle is the tensor product

$$\mathcal{H} = \mathscr{H} \otimes \mathbb{C}^d, \tag{2}$$

where \mathcal{H} is the countably infinite dimensional Hilbert space corresponding to the energy of the particle, and \mathbb{C}^d is the d-dimensional space associated with its spin. For a spin-j particle, the spin space dimension is d=2j+1. An orthonormal basis for \mathcal{H} is

$$B_{\mathscr{H}} = \left\{ |n\rangle \,\middle|\, n \in \mathbb{N}_0 \right\}. \tag{3}$$

where $\{|n\rangle\}$ represents energy eigenstates. For a spin-1/2 particle, an orthonormal basis for \mathbb{C}^2 is

$$B_{\mathbb{C}^2} = \{ |0\rangle := |\uparrow\rangle, |1\rangle := |\downarrow\rangle \},\tag{4}$$

so the total Hilbert space for a single particle, Eq. (2), has an orthonormal basis

$$B_{\mathcal{H}} = \left\{ |n\rangle \otimes |m\rangle \,\middle|\, n \in \mathbb{N}_0, m \in \{0, 1\} \right\}. \tag{5}$$

Consequently, the total state space for two distinguishable spin-1/2 particles is $\mathcal{H}^{\otimes 2} = \mathscr{H}^{\otimes 2} \otimes (\mathbb{C}^2)^{\otimes 2}$, with an orthonormal basis

$$B_{\mathcal{H}^{\otimes 2}} = \left\{ |n_1, n_2\rangle \otimes |m_1, m_2\rangle \, \middle| \, n_i \in \mathbb{N}_0, m_i \in \{0, 1\}, i = 1, 2 \right\}.$$
(6)

If the particles are *indistinguishable* fermions their collective state, $|\Psi\rangle$, must be antisymmetric under particle exchange, i.e., it belongs to the totally antisymmetric subspace $|\Psi\rangle \in \mathcal{H}^{(\mathrm{Alt})} \subset \mathcal{H}^{\otimes 2}$. With respect to the spaces $\mathscr{H}^{\otimes 2}$ and $(\mathbb{C}^2)^{\otimes 2}$, the antisymmetric subspace decomposes into a direct sum in the following fashion

$$\mathcal{H}^{(\mathrm{Alt})} = \left(\left[\mathscr{H}^{\otimes 2} \right]^{(\mathrm{Sym})} \otimes \left[\left(\mathbb{C}^{2} \right)^{\otimes 2} \right]^{(\mathrm{Alt})} \right)$$

$$\oplus \left(\left[\mathscr{H}^{\otimes 2} \right]^{(\mathrm{Alt})} \otimes \left[\left(\mathbb{C}^{2} \right)^{\otimes 2} \right]^{(\mathrm{Sym})} \right),$$

$$(7)$$

where

$$\left[\left(\mathbb{C}^{2} \right)^{\otimes 2} \right]^{(\mathrm{Sym})} = \operatorname{span} \left\{ \left| 00 \right\rangle, \left| 01 \right\rangle + \left| 10 \right\rangle, \left| 11 \right\rangle \right\},
\left[\left(\mathbb{C}^{2} \right)^{\otimes 2} \right]^{(\mathrm{Alt})} = \operatorname{span} \left\{ \left| 01 \right\rangle - \left| 10 \right\rangle \right\},$$
(8)

are the familiar triplet and singlet subspaces respectively, and

$$\left[\mathcal{H}^{\otimes 2}\right]^{(\mathrm{Sym})} = \operatorname{span}\left\{\left|n-k,k\right\rangle + \left|k,n-k\right\rangle, 0 \le k \le \left\lfloor\frac{n}{2}\right\rfloor\right\},$$

$$\left[\mathcal{H}^{\otimes 2}\right]^{(\mathrm{Alt})} = \operatorname{span}\left\{\left|n-k,k\right\rangle - \left|k,n-k\right\rangle, 0 \le k \le \left\lceil\frac{n}{2}\right\rceil - 1\right\},$$
(9)

are the symmetric and antisymmetric spaces corresponding to the energy eigenbasis. Note that we have used the shorthand $|k, n-k\rangle := |k\rangle \otimes |n-k\rangle$ for two-particle states of total energy n.

Thus, the energetic and spin degrees of freedom of two spin-1/2 fermions combine such that if the energetic degrees of freedom are symmetric under particle exchange, then the spin degrees of freedom are antisymmetric, and vice versa. Note that a similar argument would apply to bosons. In this case, their collective state belongs to the totally symmetric subspace $\mathcal{H}^{(\mathrm{Sym})} \subset \mathcal{H}^{\otimes 2}$, such that the energy and spin degrees of freedom are either both symmetric or antisymmetric under particle exchange.

Suppose we trace over one degree of freedom of the two-particle system. The state for the remaining degree of freedom would then be an incoherent mixture of states that are either totally symmetric or antisymmetric, i.e., for $|\Psi\rangle \in \mathcal{H}^{(\mathrm{Alt})}$

$$\rho = \operatorname{Tr}_{\mathbb{C}^2} |\Psi\rangle\langle\Psi| = p\rho^{(\operatorname{Sym})} + (1 - p)\rho^{(\operatorname{Alt})}, \tag{10}$$

where $\operatorname{Tr}_{\mathbb{C}^2}$ indicates that we have traced over the spin degrees of freedom, and $\rho^{(\operatorname{Sym})} \in \mathcal{B}\{[\mathcal{H}^{\otimes 2}]^{(\operatorname{Sym})}\}$, $\rho^{(\operatorname{Alt})} \in \mathcal{B}\{[\mathcal{H}^{\otimes 2}]^{(\operatorname{Alt})}\}$. Here, $\mathcal{B}(\mathcal{H})$ indicates the space of bounded linear operators acting on a Hilbert space \mathcal{H} with finite Hilbert-Schmidt norm (see [36, 37] for further details). Thus, by carefully engineering the joint spin state of two particles, we can control the probability, p, with which their energy degrees of freedom are symmetric (resp. antisymmetric) under particle exchange. This results in a continuous interpolation between bosonic and fermionic statistics giving rise to so-called statistical anyons [22].

The above scenario can be generalized to the case of N particles. The total state space $\mathcal{H}^{\otimes N} = \mathcal{H}^{\otimes N} \otimes (\mathbb{C}^d)^{\otimes N}$ can be decomposed into subspaces according to the various symmetries of the collective state of the particles under exchange, see App. A. If the particles are bosons (resp. fermions) then the totally symmetric (resp. anti-

symmetric) subspaces block-diagonalize as

$$\mathcal{H}^{(\operatorname{Sym})} = \left(\left[\mathscr{H}^{\otimes N} \right]^{(\operatorname{Sym})} \otimes \left[\left(\mathbb{C}^{d} \right)^{\otimes N} \right]^{(\operatorname{Sym})} \right)$$

$$\oplus \left(\left[\mathscr{H}^{\otimes N} \right]^{(\operatorname{Alt})} \otimes \left[\left(\mathbb{C}^{d} \right)^{\otimes N} \right]^{(\operatorname{Alt})} \right)$$

$$\oplus \tilde{\mathcal{H}}^{(\operatorname{Sym})}, \tag{11}$$

$$\mathcal{H}^{(\operatorname{Alt})} = \left(\left[\mathscr{H}^{\otimes N} \right]^{(\operatorname{Sym})} \otimes \left[\left(\mathbb{C}^{d} \right)^{\otimes N} \right]^{(\operatorname{Alt})} \right)$$

$$\oplus \left(\left[\mathscr{H}^{\otimes N} \right]^{(\operatorname{Alt})} \otimes \left[\left(\mathbb{C}^{d} \right)^{\otimes N} \right]^{(\operatorname{Sym})} \right)$$

$$\oplus \tilde{\mathcal{H}}^{(\operatorname{Alt})}, \tag{12}$$

see Eq. (A27) in App. A 2. Here, $\tilde{\mathcal{H}}^{(\mathrm{Sym})}$, $\tilde{\mathcal{H}}^{(\mathrm{Alt})}$ correspond to the product spaces of non-trivial symmetries which, when multiplied, give rise to totally symmetric and antisymmetric spaces respectively. Specifically, the dimensions of $[(\mathbb{C}^d)^{\otimes N}]^{(\mathrm{Sym})}$, and $[(\mathbb{C}^d)^{\otimes N}]^{(\mathrm{Alt})}$ are given by

$$\dim \left[\left(\mathbb{C}^d \right)^{\otimes N} \right]^{(\operatorname{Sym})} = \binom{d+N-1}{N},$$

$$\dim \left[\left(\mathbb{C}^d \right)^{\otimes N} \right]^{(\operatorname{Alt})} = \binom{d}{N}.$$
(12)

Note that if d < N, the antisymmetric subspace has dimension zero, meaning that it is not possible to construct a normalizable antisymmetric state. Just as in the two particle case, we can interpolate between bosonic and fermionic behavior of the energy degrees of freedom by controlling the auxiliary degrees of freedom associated with \mathbb{C}^d . In the following section, we will see how this control can be achieved via an energetic bias towards (or against) symmetric states of $(\mathbb{C}^d)^{\otimes N}$.

III. THERMODYNAMICS OF HAMILTONIAN ANYONS

In this section, we study the key thermodynamic properties of Hamiltonian anyons. We first derive the partition function and internal energy for an N-particle anyonic system subject to a Harmonic oscillator potential, demonstrating that such a system exhibits non-trivial first and second-order phase transitions. We later compare and contrast Hamiltonian anyons with the statistical anyons, as described in Ref. [22].

A. Partition function and internal energy

We consider a system of identical, non-interacting fermions in a one-dimensional harmonic trap with a symmetry-dependent energy bias as described by the following Hamiltonian

$$H = H_{\mathrm{HO}} \otimes \mathbb{I}_{(\mathbb{C}^d)^{\otimes N}} + \mathbb{I}_{\mathscr{H}^{\otimes N}} \otimes \nu \Pi_{(\mathbb{C}^d)^{\otimes N}}^{(\mathrm{Alt})} + \mu \tilde{\Pi}. \quad (13)$$

Here, $H_{\rm HO}$ denotes the Hamiltonian for a one-dimensional harmonic oscillator with N particles; $\Pi_{(\mathbb{C}^d)^{\otimes N}}^{({\rm Alt})}$ is the projector onto the antisymmetric subspace, $[(\mathbb{C}^d)^{\otimes N}]^{({\rm Alt})}$; and $\tilde{\Pi}$ is the projector onto $\tilde{\mathcal{H}}$, the product space of nontrivial symmetries. The parameter ν acts as an energy penalty for antisymmetric states of the auxiliary degree of freedom. Similarly, the role of parameter μ is to penalize mixed-symmetry states. Here and throughout, we take μ to be much larger than any other energy scale in the system such that the population of $\tilde{\mathcal{H}}$ can be entirely neglected. It will be assumed that when the system is weakly coupled to a large heat bath at inverse temperature β , it thermalizes to the Gibbs state $\tau = \frac{1}{Z}e^{-\beta H}$ [26], with $Z = {\rm Tr}[e^{-\beta H}]$ the partition function.

As the overall state space belongs to $\mathcal{H}^{(Alt)}$, Eq. (11), the projection of the Hamiltonian onto this space is

$$H^{(\mathrm{Alt})} = H_{\mathrm{HO}}^{(\mathrm{Alt})} \otimes \Pi_{(\mathbb{C}^d)^{\otimes N}}^{(\mathrm{Sym})} + [H_{\mathrm{HO}} + \nu \mathbb{I}_{\mathscr{H}^{\otimes N}}]^{(\mathrm{Sym})} \otimes \Pi_{(\mathbb{C}^d)^{\otimes N}}^{(\mathrm{Alt})} + \mu \tilde{\Pi}^{(\mathrm{Alt})}.$$
(14)

As the three terms of $H^{(\mathrm{Alt})}$ in Eq. (14) act on mutually orthogonal subspaces, the Hamiltonian can straightforwardly be exponentiated as

$$\left[e^{-\beta H}\right]^{(\mathrm{Alt})} = \left[e^{-\beta H_{\mathrm{HO}}}\right]^{(\mathrm{Alt})} \otimes \Pi_{(\mathbb{C}^{d})^{\otimes N}}^{(\mathrm{Sym})}
+ e^{-\beta \nu} \left[e^{-\beta H_{\mathrm{HO}}}\right]^{(\mathrm{Sym})} \otimes \Pi_{(\mathbb{C}^{d})^{\otimes N}}^{(\mathrm{Alt})},$$
(15)

where the mixed-symmetry term $e^{-\beta\mu}\tilde{\Pi}^{(\mathrm{Alt})}$ has been neglected because $\beta\mu\gg 1$. Taking the trace of Eq. (15) we obtain the partition function

$$Z = {d + N - 1 \choose N} Z_{\rm F} + {d \choose N} e^{-\beta \nu} Z_{\rm B}, \qquad (16)$$

where the binomial prefactors are the dimensions of $[(\mathbb{C}^d)^{\otimes N}]^{(\mathrm{Alt})}$ and $[(\mathbb{C}^d)^{\otimes N}]^{(\mathrm{Sym})}$ respectively. Equation 16 is a linear combination of the partition functions for N non-interacting fermions or bosons in a harmonic potential, $Z_{\mathrm{F/B}} = \mathrm{Tr}\{[e^{-\beta H_{\mathrm{HO}}}]^{(\mathrm{Alt/Sym})}\}$. The explicit expression of these are

$$Z_{\rm F} = e^{-\beta\hbar\omega \frac{N^2}{2}} \prod_{k=1}^{N} \frac{1}{1 - e^{-\beta\hbar\omega k}},$$

$$Z_{\rm B} = e^{-\beta\hbar\omega \frac{N}{2}} \prod_{k=1}^{N} \frac{1}{1 - e^{-\beta\hbar\omega k}},$$
(17)

where ω is the fundamental frequency of the oscillator [38, 39]. Tracing out the auxiliary degree of freedom one obtains the reduced thermal state, $\tau_{\mathcal{H}^{\otimes N}}$, of the harmonic oscillator degrees of freedom, which is a mixture of the fermionic and bosonic thermal states

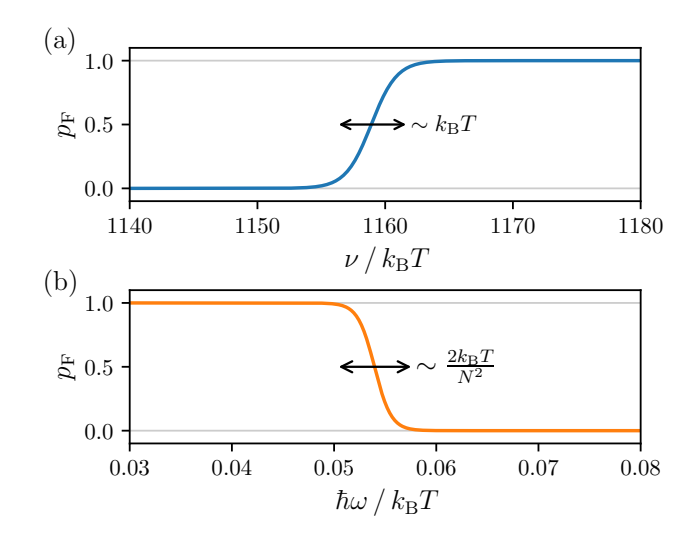


FIG. 2. The fermionic subspace overlap, $p_{\rm F}$, plotted as a function of ν/k_BT in panel (a) and $\hbar\omega/k_BT$ in panel (b). The system undergoes a transition from bosonic to fermionic statistics, as described by Eq. (19). In panel (a) we set $\hbar\omega=k_{\rm B}T$, and the characteristic width of the sigmoid curve is $k_{\rm B}T$. In panel (b) we set $\nu=0$; and the width of the transition is $\sim 2k_{\rm B}T/N^2$, becoming vanishingly narrow for large N. In both panels we have taken N=d=50. Note the inflection point at $p_{\rm F}=1/2$.

$$\tau_{\mathrm{F/B}} = \frac{1}{Z_{\mathrm{F/B}}} \left[e^{-\beta H_{\mathrm{HO}}} \right]^{(\mathrm{Alt/Sym})}$$

$$\tau_{\mathcal{H}^{\otimes N}} = \binom{d+N-1}{N} \frac{Z_{\mathrm{F}}}{Z} \tau_{\mathrm{F}} + \binom{d}{N} e^{-\beta \nu} \frac{Z_{\mathrm{B}}}{Z} \tau_{\mathrm{B}}$$

$$= p_{\mathrm{F}} \tau_{\mathrm{F}} + (1-p_{\mathrm{F}}) \tau_{\mathrm{B}}, \qquad (18)$$

where the parameter $p_{\rm F} \in [0,1]$ reads

$$p_{\rm F} = \frac{1}{1 + \exp\left[\frac{1}{2}N(N-1)\beta\hbar\omega - \beta\nu - h(d,N)\right]}, \quad (19)$$

and we have defined the shorthand $h(d,n):=\ln\binom{d+N-1}{N}-\ln\binom{d}{N}$ in the exponential. The parameter $p_{\rm F}$ encapsulates the state's overlap with the antisymmetric subspace, interpolating from fully bosonic $(p_{\rm F}=0)$ to fermionic $(p_{\rm F}=1)$ as ν is varied. Figure 2 shows the strictly monotonic behavior of $p_{\rm F}$ with respect to parameters ω and ν

The fermionic overlap $p_{\rm F}$ plays a crucial role also for the internal energy of the system. For an arbitrary state ρ , the internal energy is given by the expectation value of the Hamiltonian, $U = \text{Tr}[H^{(\text{Alt})}\rho]$, where $H^{(\text{Alt})}$ as in Eq. (14). In the specific case of a thermal state, $U = -\frac{\partial \ln Z}{\partial \beta}$ [40], and using Eq. (16), we obtain

$$U = p_{\rm F} U_{\rm F} + (1 - p_{\rm F}) \left(\nu + U_{\rm B}\right), \tag{20}$$

where the internal energies for bosons and fermions read

$$U_{\rm F} = \hbar\omega \frac{N^2}{2} + \sum_{k=1}^{N} \frac{k\hbar\omega}{e^{k\beta\hbar\omega} - 1},$$

$$U_{\rm B} = \hbar\omega \frac{N}{2} + \sum_{k=1}^{N} \frac{k\hbar\omega}{e^{k\beta\hbar\omega} - 1},$$
(21)

as shown in Ref. [38]. Observe that $U_{\rm F}$ and $U_{\rm B}$ differ only in the ground state term. The difference corresponds to the fact that all N bosons can occupy the harmonic oscillator ground state at energy $\hbar\omega/2$, whereas fermions must fill successive levels due to Pauli exclusion. For large N, and at low temperatures, the internal energies radically differ, a phenomenon sometimes referred to as $Pauli\ energy\ [35]$.

B. Phase transitions

We have seen that the internal energy of the N-particle ground state exhibits radically different scaling depending on exchange symmetry. One would therefore anticipate an abrupt change in the internal energy of Hamiltonian anyons at the transition between fermionic and bosonic statistics as characterized by the change in $p_{\rm F}$, the overlap with the fermionic subspace. In this subsection, we demonstrate that the fermion-boson crossover constitutes a bona fide phase transition. A k-th order phase transition is characterized by a non-analyticity in the k-th derivative of the internal energy [41].

As seen in Fig. 2, $p_{\rm F}$ takes the form of a sigmoid curve centered at $p_{\rm F}=1/2$, where the parameters β,ω and ν satisfy

$$\phi := \frac{1}{2}N(N-1)\beta\hbar\omega - \beta\nu - h(d,N) = 0.$$
 (22)

To check for phase transitions, we compute the first and second derivatives of internal energy, Eq. (20), with respect to T, ω, ν , at the point where $p_F = 1/2$, see App. C. In the thermodynamic limit, $N \to \infty$, we find that the thermal capacities, $C_X = \partial U/\partial X$, $X \in \{T, \omega, \nu\}$, are given by

$$\lim_{N \to \infty} \frac{1}{N^2} C_T = k_{\rm B} \lim_{N \to \infty} \frac{h(d, N)^2}{4N^2},$$

$$\lim_{N \to \infty} \frac{1}{N^2} C_{\nu} = \lim_{N \to \infty} \frac{h(d, N)}{4N^2},$$

$$\lim_{N \to \infty} \frac{1}{N^2} C_{\omega} = \frac{\hbar}{4} - \frac{\hbar}{2} \lim_{N \to \infty} h(d, N).$$
(23)

Note that the division by N^2 is necessary in order for the system to have a finite energy density in the thermodynamic limit. Observe that C_{ω}/N^2 diverges, whilst C_T/N^2 and C_{ν}/N^2 remain bounded, see Eq. (C13) in App. C6 for the limiting behavior of h(d,N). Thus, the system undergoes a first-order phase transition as the trap frequency ω is varied.

The second derivatives of the internal energy can be shown to vanish at the inflection point $p_{\rm F}=1/2$. However, by examining the behavior of the second derivatives ε close on either side of that point, we find the following limiting behavior

$$\lim_{N \to \infty} \frac{1}{N^2} \frac{\partial^2 U}{\partial T^2} = \lim_{N \to \infty} \frac{\varepsilon k_{\rm B}}{8T} \frac{\left[h(d, N) + \varepsilon\right]^3}{N^2} + \frac{1}{N^2} \frac{\partial^2 U_{\rm B}}{\partial \beta^2}$$

$$\lim_{N \to \infty} \frac{1}{N^2} \frac{\partial^2 U}{\partial \nu^2} = \lim_{N \to \infty} \frac{\varepsilon \beta}{8} \left[\frac{h(d, N) + \varepsilon}{N^2} \right] - \frac{\beta}{2N^2}. \quad (24)$$

As the second derivative with respect to temperature clearly diverges, it follows that the system experiences a second-order phase transition as the temperature is varied. Note, however, that no phase transition arises for the symmetry bias, ν .

Figure 3 shows the specific heat per particle, $c_X = \frac{1}{N} \frac{\partial U}{\partial X}$, with $X \in \{T, \omega\}$ where we can clearly identify two regimes—determined by the relation between T, ν and ω at $p_{\rm F} = 1/2$ —marked with an abrupt change in the specific heat. Note that this is a symmetry-driven phase transition similar to Bose-Einstein condensation or symmetry-breaking dynamical phase transitions [42, 43].

C. Comparison between Hamiltonian and statistical anyons

In this subsection, we compare the thermal properties of Hamiltonian anyons with the statistical anyons proposed in [22]. Statistical anyons are based on an ensemble of noninteracting identical particles pairs whose symmetry can be manipulated, as in a Hong-Ou-Mandel effect [44]. For an ensemble composed of $N_{\rm F}$ fermionic systems and $N_{\rm B}$ bosonic ones, the properties of the system are characterized by the ratio $k_{\rm F} = \frac{N_{\rm F}}{N_{\rm F} + N_{\rm B}}$. In particular, the partition function $Z_{\rm SA}$ and internal energy $U_{\rm SA}$ for an ensemble of statistical anyon pairs are given by

$$Z_{SA} = (Z_F)^{k_F} (Z_B)^{(1-k_F)},$$

$$U_{SA} = k_F U_F + (1 - k_F) U_B,$$
(25)

where $Z_{\rm F/B}$ and $U_{\rm F/B}$ are defined in the previous section, see Eq. (21). These equations contrast with their equivalent for Hamiltonian anyons, Eqs. (16) and (20).

Both Hamiltonian and statistical anyons have similar thermodynamic properties, with $p_{\rm F}$ and $k_{\rm F}$ playing a similar role. The main difference between the two models is the dynamic character of Hamiltonian anyons, as the parameter $p_{\rm F}$ depends on the variables ω, ν and β , in contrast to statistical anyons where $k_{\rm F}$ is fixed. We shall see in Section IV that the adaptive nature of Hamiltonian anyons confers novel advantages for heat engines.

In Fig. 4, we compare the internal energy, Fig. 4(a), and heat capacity (C_T) , Fig. 4(b), for statistical and Hamiltonian anyons as well as for bosons and fermions, as a function of temperature. The comparison is made

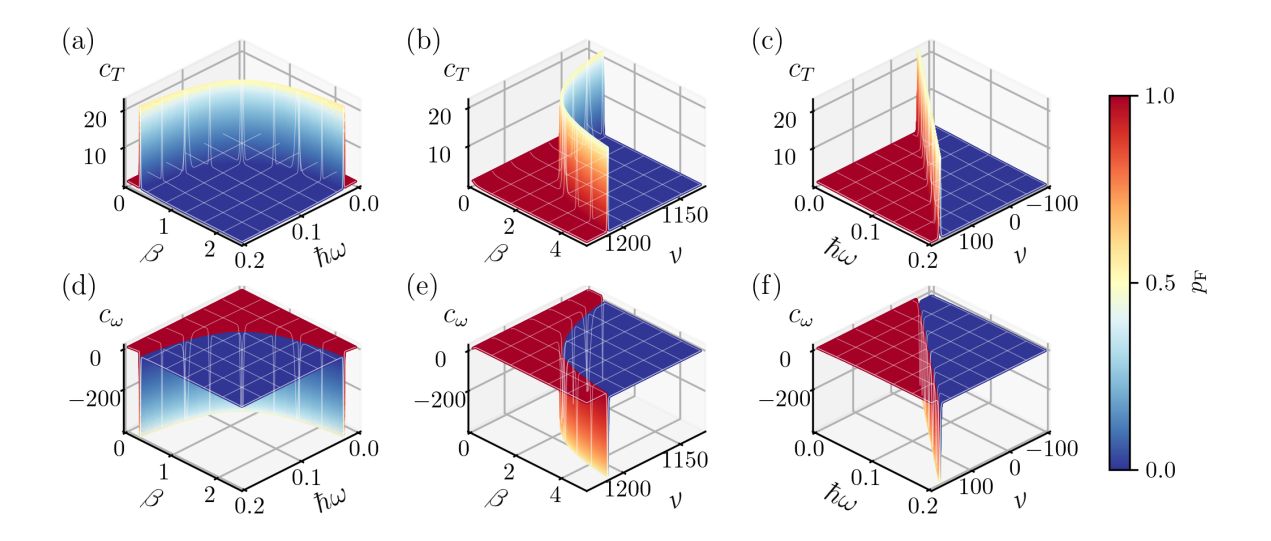


FIG. 3. Diagrams of the heat capacity per particle, c_T (panels (a)–(c)), and c_ω (panels (d)–(f)) for N=d=50. The energies are in arbitrary units. Note that for ω , there is an order of magnitude bigger jump in the derivative of U than for T. The jump follows the expression given by Eq. (22) with $\varepsilon=0$, corresponding to equal overlap with the fermionic and bosonic subspaces.

for $k_F = 0.5$ and $\nu = 0$. The general trend of the system energy is the same for all cases, increasing when T increases or when ω decreases. The behavior of both Hamiltonian and statistical anyons interpolates between that of purely bosonic and fermionic ensembles. However, due to their dynamical nature, and the presence of non-trivial phase transitions, Hamiltonian anyons exhibit a much higher heat capacity that of all other mediums. This phenomenon can be exploited for the construction of engines with increased efficiency and power as we now demonstrate.

IV. QUANTUM ENGINES BASED ON SYMMETRY CONTROL

Particle exchange symmetry is known to affect the performance of heat engines at low temperatures [22, 34], and work extraction cycles based on manipulating particle statistics have recently been demonstrated in ultracold gases [35]. In this section we demonstrate how the ability to dynamically vary the statistical properties of Hamiltonian anyons can be exploited for novel advantages in quantum heat engines. Two types of cycle will be considered: a Stirling cycle in which the conventional compression and expansion strokes are replaced by fermionization and bosonization of the working medium (Sec. IV A), and a finite-time Otto cycle where the medium passively transitions between fermionic and bosonic statistics during heating and cooling (Sec. IV B).

Before analyzing the performance of these cycles, let us briefly review some basic concepts from quantum thermodynamics and define the notions of heat and work that we will use. We assume that parameters ω and ν can be

externally controlled, and that the system may be connected at different times with different heat baths, each characterized by an inverse temperature β .

The cycles considered here each consist of two driving strokes and two thermalization strokes. During a driving stroke, either ω or ν is varied, causing the system to evolve according to a time-dependent Hamiltonian while in contact with a fixed-temperature bath. Conversely, in a thermalization stroke, the system is disconnected from one heat bath and connected to another, whereupon it is allowed to equilibrate to the Gibbs state at the new temperature, with the Hamiltonian remaining fixed throughout.

The rates of work and heat transfer will be defined according to [28]

$$\dot{W} = -\text{Tr}\left(\rho\dot{H}\right),$$

$$\dot{Q} = \text{Tr}\left(\dot{\rho}H\right),$$
(26)

using the convention that positive work is done by the system against the driving field, and positive heat is absorbed into the system from the bath. We note that these definitions are consistent with the first law of thermodynamics, $\dot{U} = \dot{Q} - \dot{W}$ [24, 26, 27].

During the thermalization strokes, the Hamiltonian is unchanging, i.e., $\dot{H}=0$, so changes to the internal energy of the system are purely heat. During driving strokes, the work and heat depend on how the stroke is performed. In order to simplify the analysis we shall consider two idealized driving schemes: adiabatic fast driving and quasistatic isothermal driving. In adiabatic fast driving, the Hamiltonian is switched from H_i to H_f much faster than the system's evolution, so that the state remains unchanged, i.e., $\dot{\rho}=0$. Consequently, Q=0 and the

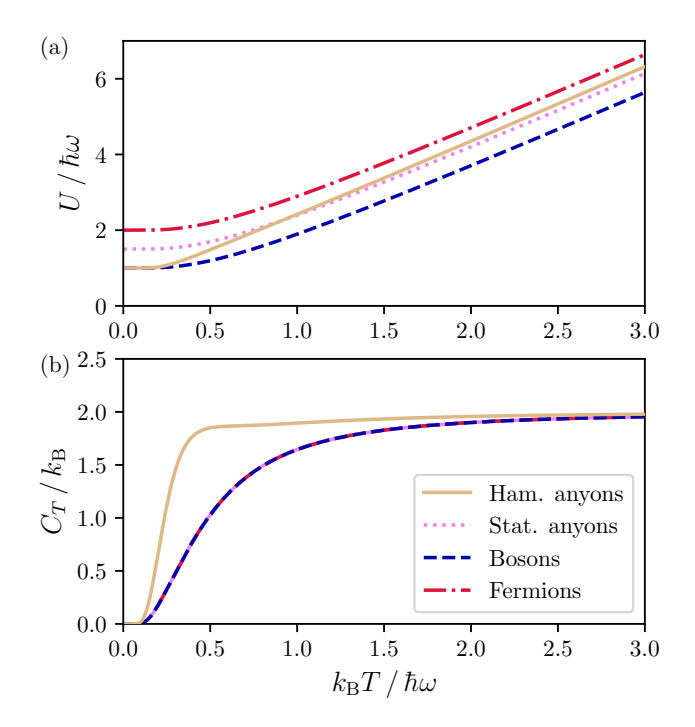


FIG. 4. Internal energy (a) and heat capacity (b) as a function of temperature, for a pair of fermions, bosons, statistical anyons with $k_{\rm F}=0.5$, and Hamiltonian anyons with $\nu=0$. Statistical anyons are described by a fixed-weighting mean of fermions and bosons (which have identical heat capacities). Note that the pink, dotted line representing statistical anyons overlaps with the lines for bosons and fermions in panel (b). The internal energy of Hamiltonian anyons interpolates according to the temperature-dependent weighting $p_{\rm F}$. This additional temperature dependence means that the heat capacity of Hamiltonian anyons can exceed that of fermions and bosons. These plots are for the case N=2, d=2.

change in internal energy of the system is purely work, $W = \text{Tr}(\rho H_i) - \text{Tr}(\rho H_f)$. On the other hand, in quasistatic isothermal driving, the Hamiltonian is changed from H_i to H_f at a rate which is slow in comparison to thermalization, resulting in the system remaining in the instantaneous Gibbs state $\tau[\beta, H(t)]$ at all times. In this case work is equal to the change in free energy, i.e.

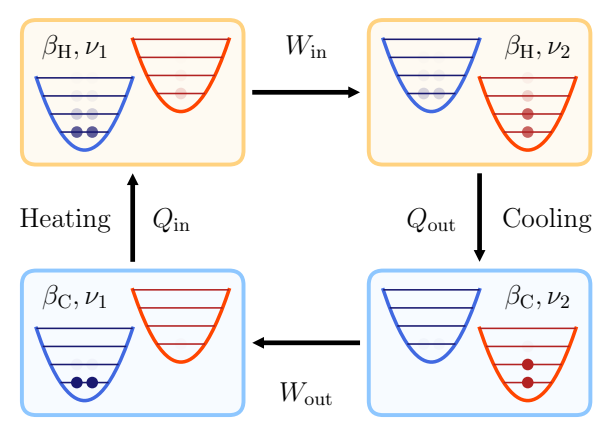
$$W = \frac{1}{\beta} \ln \left[\frac{Z(\beta, H_f)}{Z(\beta, H_i)} \right], \tag{27}$$

where the partition function Z is as in Eq. (16). This is accompanied by a nontrivial heat transfer, which can be determined using the first law as $Q = U(\beta, H_f) - U(\beta, H_i) + W$.

A. Stirling Cycle

In a classical heat engine, a piston varies the volume of a cylinder of gas in order to extract useful work. A quantum equivalent would vary the fundamental frequency ω

Isothermal fermionization



Isothermal bosonization

FIG. 5. Schematic diagram of a modified Stirling cycle based on fermionizing and bosonizing the particle statistics. A pair of Hamiltonian anyons has access to two ladders of energy eigenstates, one with bosonic exchange symmetry (blue) and one fermionic (red), which are offset by a variable energy bias ν . As both particles can occupy the bosonic ground state, the internal energy is lower than for fermions which are subject to Pauli exclusion. By lowering ν , so that the particles have access to bosonic states, energy can be extracted as work. Moreover, by bosonizing at one temperature and fermionizing at another, a net output of work can be achieved in a cycle.

of the confining potential [31, 33, 45, 46]. Instead, we here consider actively driving the statistical properties of a medium of Hamiltonian anyons via the parameter ν , as shown in Fig. 5, while holding ω fixed throughout. Starting in a thermal state at temperature $\beta_{\rm H}$ and $\nu = \nu_1$, the parameter ν is quasistatically and isothermally driven to ν_2 while the system remains in equilibrium with the hot bath. The system is then connected to the cold bath and thermalizes to $\beta_{\rm C}$ with ν fixed. The parameter ν is then isothermally driven back to $\nu = \nu_1$, and finally the cycle is completed by allowing the system to thermalize with the hot bath at $\beta_{\rm H}$.

In general, when the bias is isothermally driven from ν_i to ν_f , the work extraction is given by

$$W = \frac{1}{\beta} \ln \left[\frac{p_{\rm F}(\beta, \nu_i)}{p_{\rm F}(\beta, \nu_f)} \right], \tag{28}$$

where we have used the fact that $p_{\rm F} = \binom{d+N-1}{N} \frac{Z_{\rm F}}{Z}$ with $Z_{\rm F}$ independent of ν . Eq. (28) makes evident the strikingly direct relationship between thermodynamic work and the change in particle exchange symmetry, as characterized by $p_{\rm F}$. As $p_{\rm F}$ is a monotonically increasing function of ν (see Fig. 2), lowering ν (bosonizing) necessarily results in positive work extraction, while raising ν (fermionizing) constitutes work done on the system. See caption of Fig. 5 a the physical interpretation.

The net work extraction during the cycle is given by

summing both isothermal strokes

$$W_{\text{cyc}} = \frac{1}{\beta_{\text{H}}} \ln \left[\frac{p_{\text{F}}(\beta_{\text{H}}, \nu_1)}{p_{\text{F}}(\beta_{\text{H}}, \nu_2)} \right] + \frac{1}{\beta_{\text{C}}} \ln \left[\frac{p_{\text{F}}(\beta_{\text{C}}, \nu_2)}{p_{\text{F}}(\beta_{\text{C}}, \nu_1)} \right]. \tag{29}$$

Due to the non-trivial temperature dependence of $p_{\rm F}$, $W_{\rm cyc}$ is not guaranteed to be positive, and the different regimes of the cycle's usefulness are represented in Fig. 6. Rather remarkably, it can be advantageous to perform the work extraction stroke at the colder isotherm, as discussed in Appendix D.

A key metric of performance is the cycle's thermodynamic efficiency, given by $\eta = W_{\rm cyc}/Q_{\rm H}$, where $Q_{\rm H}$ is the net heat absorbed from the hot bath. By considering the total change of internal energy and work done while in contact with the hot bath, we can write an expression for $Q_{\rm H}$ using the first law

$$Q_{\rm H} = U(\beta_{\rm H}, \nu_2) - U(\beta_{\rm C}, \nu_1) + \frac{1}{\beta_{\rm H}} \ln \left[\frac{p_{\rm F}(\beta_{\rm H}, \nu_1)}{p_{\rm F}(\beta_{\rm H}, \nu_2)} \right], (30)$$

where U is given by Eq. (20). Figure 6 shows a plot of efficiency as a function of the parameters ν_1, ν_2 .

In the limiting cases $p_{\rm F}(\beta, \nu_2) \to 1$ and $p_{\rm F}(\beta, \nu_1) \to 0$, where ν is driven though a sufficiently large range of values for *complete* fermionization and bosonization, the net work and heat of the cycle are (see App. D)

$$W_{\text{cyc}} \to \left(\frac{1}{\beta_{\text{H}}} - \frac{1}{\beta_{\text{C}}}\right) h(d, N),$$

$$Q_{\text{H}} \to \frac{1}{\beta_{\text{H}}} h(d, N) + \sum_{k=1}^{N} \left(\frac{k\hbar\omega}{e^{k\beta_{\text{H}}\hbar\omega} - 1} - \frac{k\hbar\omega}{e^{k\beta_{\text{C}}\hbar\omega} - 1}\right).$$
(31)

Under the further assumption that $\beta\hbar\omega \gg 1$ for both temperatures (i.e. in very cold regimes where particle statistics matter the most), the second term in $Q_{\rm H}$ vanishes, and the cycle attains the ideal Carnot efficiency

$$\eta \to 1 - \frac{\beta_{\rm H}}{\beta_{\rm C}}.$$
 (32)

Additionally, there exist regions of ν_1 and ν_2 for which $W_{\rm cyc} \leq 0$ where the cycle acts as a refrigerator, absorbing a net positive amount of heat $Q_{\rm C}$ from the cold bath. For such cases, the coefficient of performance $Q_{\rm C}/|W_{\rm cyc}|$ is plotted as a function of ν_1 and ν_2 in Fig. 6.

B. Finite-time Otto cycle

Here, we consider a fast-switching Otto cycle which involves a temperature-induced transition in a working substance of Hamiltonian anyons. Unlike the Stirling engine, the strokes in an Otto cycle occur in finite time, allowing us to study possible enhancements to an engine's *power*. The cycle acts between two heat baths at temperatures $\beta_{\rm H} < \beta_{\rm C}$ with the strokes implemented by varying the frequency of the trap as shown in Fig. 7.

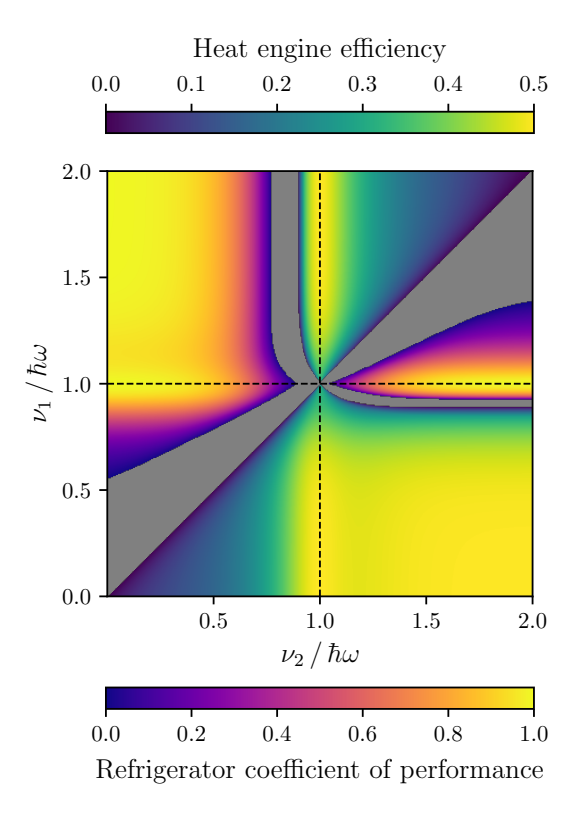


FIG. 6. Performance of a modified Stirling cycle with a pair of Hamiltonian anyons as a working substance (N=d=2). All energies are in units of $\hbar\omega$, which remains fixed throughout the cycle, and the bath inverse-temperatures are $\beta_{\rm H}=10\hbar\omega$ and $\beta_{\rm C}=20\hbar\omega$ such that $\eta_{\rm Carnot}=0.5$. Thermodynamic efficiency is plotted in regimes where the cycle extracts positive work; and refrigerator coefficient of performance is plotted where the cycle removes heat from the cold bath. In the upper-right and bottom-left quadrants, the engine extracts work whenever $\nu_1>\nu_2$ and $\nu_1<\nu_2$ respectively. The cycle approaches reversible efficiency in some regimes, notably in the lower-right, where the system is driven far either side of the fermion-boson transition. In the regimes which are shaded gray, the cycle functions neither as a heat engine nor a refrigerator.

Starting in the thermal state $\tau(\beta_{\rm H}, \omega_1)$, the trap frequency is quickly and adiabatically switched from ω_1 to a smaller value ω_2 —corresponding to an expansion of the confining potential—during which the state undergoes no evolution. The system is then placed in contact with a cold bath and thermalizes to $\tau(\beta_{\rm C}, \omega_2)$. Following this, the frequency is instantaneously switched back from ω_2 to ω_1 , compressing the trap, with the system remaining in the state $\tau(\beta_{\rm C}, \omega_2)$. The cycle is completed by placing the system in contact with the hot bath, allowing it to thermalize back to its original state $\tau(\beta_{\rm H}, \omega_1)$.

The value of ν remains fixed throughout, which we take to be $\nu=0$ for simplicity. Consequently, as can be seen from Eq. (13), the eigenvalues of the overall Hamiltonian are simply those of the harmonic oscillator and therefore proportional to ω . By extension, the internal energy fol-

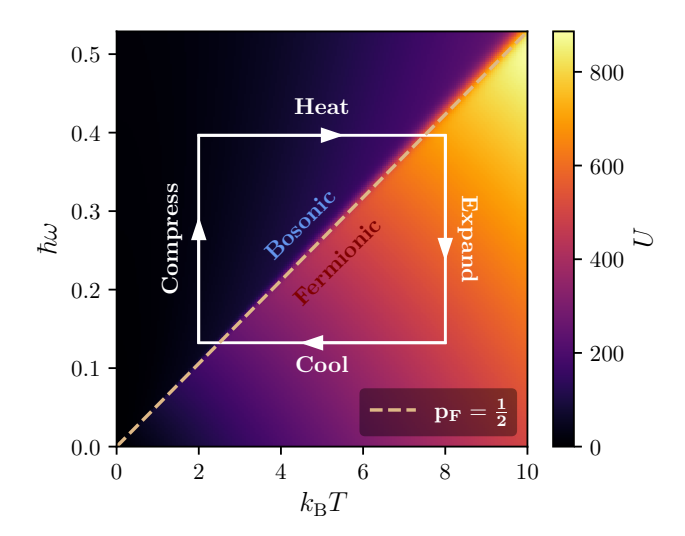


FIG. 7. Sketch of the Otto cycle, overlaid on a heatmap of internal energy U against temperature T and trap frequency ω for N=d=50 and $\nu=0$ (all energies in arbitrary units). By crossing the anyonic transition during the heating and cooling strokes, the work output during expansion can be boosted by the effective repulsion between particles in the fermionic phase; while compression is performed at reduced cost in the bosonic phase.

lowing the adiabatic expansion is simply changed by a factor ω_2/ω_1 , since the state remains fixed during driving. The work output of the expansion stroke is equal to the resulting reduction in internal energy given by $(1-\frac{\omega_2}{\omega_1})U(\beta_{\rm H},\omega_1)$, where U is as in Eq. (20). Similarly, the internal energy changes by a factor ω_1/ω_2 during the compression stroke so that the work done on the system is $(\frac{\omega_1}{\omega_2}-1)U(\beta_{\rm C},\omega_2)$. Therefore the net work extraction per cycle is

$$W_{\rm cyc} = \left(1 - \frac{\omega_2}{\omega_1}\right) U(\beta_{\rm H}, \omega_1) - \left(\frac{\omega_1}{\omega_2} - 1\right) U(\beta_{\rm C}, \omega_2). \tag{33}$$

On the other hand, the heat absorbed from the hot reservoir is equal to the increase in internal energy during the heating stroke

$$Q_{\rm H} = U(\beta_{\rm H}, \omega_1) - \frac{\omega_1}{\omega_2} U(\beta_{\rm C}, \omega_1), \tag{34}$$

which allows us to compute the efficiency $\eta = W_{\rm cyc}/Q_{\rm H}$. The same quantities can be evaluated for a working substance of pure bosons or fermions by replacing U in the above with $U_{\rm F}$ or $U_{\rm B}$ as given in Eq. (21). A comparison of work and efficiency between bosons, fermions and anyons is plotted in Fig. 8.

The work output $W_{\rm cyc}$ can be significantly boosted in a cycle operating across the anyonic phase transition. To see this, note that the contribution to the internal energy due to the ground state is $\hbar\omega N^2/2$ for fermions as opposed to $\hbar\omega N/2$ for bosons. Hence, for large N, the

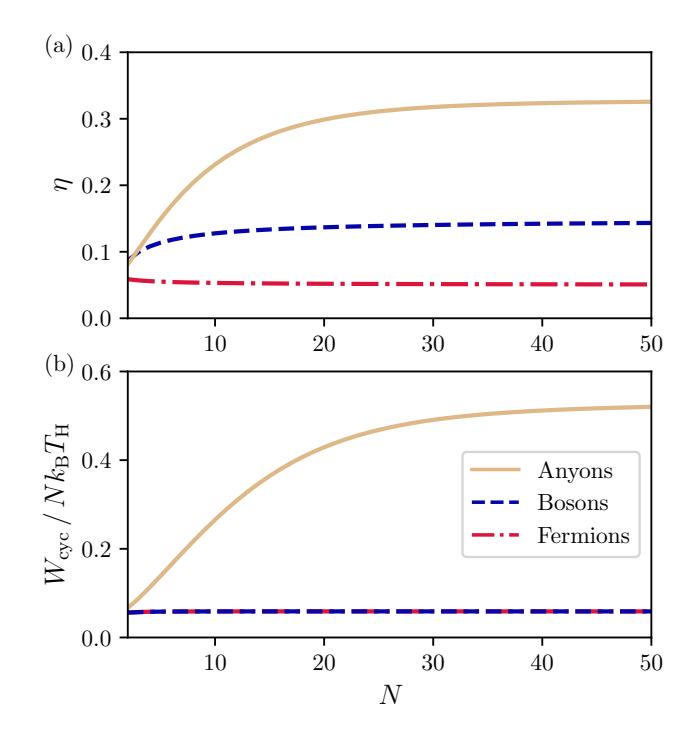


FIG. 8. Performance for a fast-switching Otto cycle with fermions, bosons, and Hamiltonian anyons as a working substance. Thermodynamic efficiency η (panel a), and work per particle per cycle $W_{\rm cyc}/Nk_{\rm B}T_{\rm H}$ (panel b) are plotted against the number of particles N in the working substance. Due to the presence of a first-order phase transition, Hamiltonian anyons outperform bosons and fermions, both in efficiency and power. The advantage becomes more pronounced as the number of particles grows. The ratio between reservoir temperatures is taken to be $\beta_{\rm C}/\beta_{\rm H}=2$ (so that the Carnot efficiency is 0.5), and the two trap frequencies are such that $\phi(\beta_{\rm H},\omega_1)=-0.1$ and $\phi(\beta_{\rm C},\omega_2)=+0.1$. In both plots d=N and $\nu=0$.

same compression ratio ω_2/ω_1 can entail a much larger work transfer for fermions than bosons. We can exploit this fact by tuning the cycle such that expansion takes place in the fermionic regime whilst compression occurs in a bosonic regime. For given reservoir temperatures $\beta_{\rm C}$ and $\beta_{\rm H}$, this situation can be engineered by choosing ω_1 and ω_2 such that $\phi(\beta_{\rm H},\omega_1)<0$ and $\phi(\beta_{\rm C},\omega_2)>0$, where ϕ is given in Eq. (22), which in turn ensures that $p_{\rm F}(\beta_{\rm C},\omega_2)\approx 0$ and $p_{\rm F}(\beta_{\rm H},\omega_1)\approx 1$ (see Fig. 7).

Figure 8 compares the efficiency, η , and power density, $W_{\rm cyc}/N$, between bosonic, fermionic and Hamiltonian anyon mediums for a fast-switching Otto engine. Unlike the statistical anyons in [22], whose performance interpolates between that of bosons and fermions, Hamiltonian anyons surpass both bosonic and fermionic working substances. The advantage can be directly attributed to the transition in particle statistics throughout the cycle, the effect of which becomes more pronounced as the number of particles of the working medium increases.

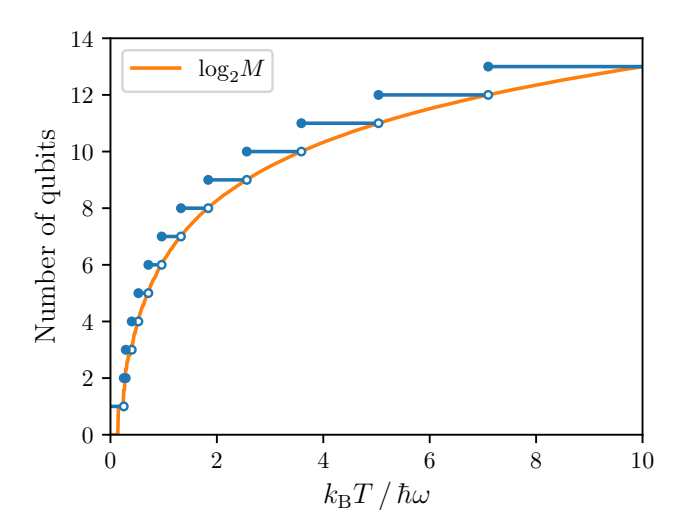


FIG. 9. Number of qubits required to represent the energy levels which account for 99.9% population in the thermal state, plotted against temperature for N=d=2. The parameter ν is adjusted so that $p_{\rm F}=1/2$ at all T values. The blue lines mark the ratio of temperature to energy that can be captured by a given integer number of qubits.

V. SIMULATION ON A QUANTUM COMPUTER

In this section, we briefly discuss how to simulate Hamiltonian anyons on digital quantum computers. The main idea is to divide the qubits of a quantum processor into two sets. A first set comprises those that are used for simulating the energy degrees of freedom, and a second one with those that are used for simulating the spin degrees of freedom. For particles with spin j, so that d = 2j + 1, the latter corresponds to $\log_2 d$ qubits. For the energy degrees of freedom, the number of qubits used depends strongly on how many eigenstates of the Harmonic oscillator we wish to simulate. Figure 9 plots the number of qubits needed to encode the energy levels that account for 99.9% of the population present in the thermal state of two particles as a function of temperature. Setting an upper bound M on the total energy eigenstates implies $\log_2 M$ qubits. Hence, to simulate Nsuch particles requires a total of $\log_2 M + N \log_2 d$ qubits.

Qubits in a quantum computer do not inherently possess the symmetry properties required for simulating Hamiltonian anyons. Hence, these have to be encoded beforehand. In Fig. 10 we show how to prepare on a quantum computer a totally antisymmetric state for the case where M=d=2, i.e., a pair of spin-1/2 particles, whose energy spectrum is limited to three distinct energy eigenvalues. The circuit consists of preparing a pair of the Bell basis states

$$|\Phi_{ij}\rangle = \left(X^i Z^j \otimes \mathbb{1}\right) \frac{1}{\sqrt{2}} \sum_{k=0}^{1} |k\rangle \otimes |k\rangle,$$
 (35)

where X and Z are the Pauli operators. Note that for i = j = 1 the state $|\Phi_{11}\rangle$ is totally antisymmetric. For each pair of Bell states the classical labels ij are imprinted onto the state of two auxiliary qubits which are then measured to produce the classical bit string $\mathbf{x} \in \{0,1\}^4$. Observe that the logical AND operator between the bits x_0 and x_1 (and likewise between bits x_2 and x_3) uniquely identifies the totally symmetric and antisymmetric states, i.e. $x_0 \wedge x_1 = 1$ if and only if the state is antisymmetric. If $x_0 \wedge x_1 \neq x_2 \wedge x_3$ then the global state of the four qubits belongs to the totally antisymmetric subspace. If, however, $x_0 \wedge x_1 = x_2 \wedge x_3$ then the states are either both symmetric or antisymmetric. In the former case (corresponding to $x_0 \wedge x_1 = 0$) we apply $X^{\bar{x}_2}Z^{\bar{x}_3}$, where \bar{x} denotes the negation of x, to the third qubit which ensures that the last two qubits in Fig. 10 are in the state $|\Phi_{11}\rangle$. If $x_0 \wedge x_1 = 1$ we simply apply X^{x_2} to the third qubit ensuring that the last two qubits in Fig. 10 are in the symmetric state $|\Phi_{10}\rangle$.

Next, we need to prepare the thermal state of Eq. (18). This is accomplished by implementing a quantum analogue of the classical Markov Chain Monte Carlo algorithm [47]. This implementation proceeds via simulation of the following dynamical operator over a generic state ρ [48]

$$\mathcal{L}_{\beta}[\rho] := -\frac{i}{\hbar} [H, \rho] + \sum_{k \in K} \int_{-\infty}^{\infty} \gamma(x) \left[\hat{L}_{k}(x) \rho \hat{L}_{k}^{\dagger}(x) - \frac{1}{2} \left\{ \hat{L}_{k}^{\dagger}(x) \hat{L}_{k}(x), \rho \right\} \right] dx, \tag{36}$$

where H is the N-particle Hamiltonian, see Eq. (13). The coefficients $\gamma(x)$ are the transition weights, which must satisfy the detailed-balance condition $\frac{\gamma(x)}{\gamma(-x)} = e^{-\beta x}$, and $\hat{L}_k(x)$ is the weighted Fourier transform of the k-th jump operator, $L_k(t)$, i.e.,

$$\hat{L}_k(x) = \frac{1}{\sqrt{2\pi}} \int_{-\infty}^{\infty} e^{-ixt} f(t) L_k(t) dt.$$
 (37)

Here f(t) is a real, square-integrable filter function and the set of jump operators $\{L_k(t)\}$ is closed under adjoints and satisfies $\|\sum_{k\in K} L_k^{\dagger}(t)L_k(t)\| \leq 1$. For a suitably chosen filter function, Ref. [48] shows that the distance between the fixpoint state of \mathcal{L}_{β} and the true thermal

state is less than
$$\mathcal{O}\left(\sqrt{\frac{\beta}{t}}t_{\text{mix}}(\mathcal{L}_{\beta})\right)$$
, where $t_{\text{mix}}(\mathcal{L}_{\beta})$ is the mixing time of the dynamics [49].

The implementation on a quantum processor proceeds by first discretizing the Fourier transform and performing a block encoding of the dynamics into a unitary operator with the help of auxiliary qubit registers (see Lemma I.1 in [48]). The resource scaling of the implementation is linear in time, and requires a bounded number of auxiliary qubit registers that depends on the block encoding, the total number K of jump operators and the discretization of the Fourier transform the latter being the most resource consuming step.

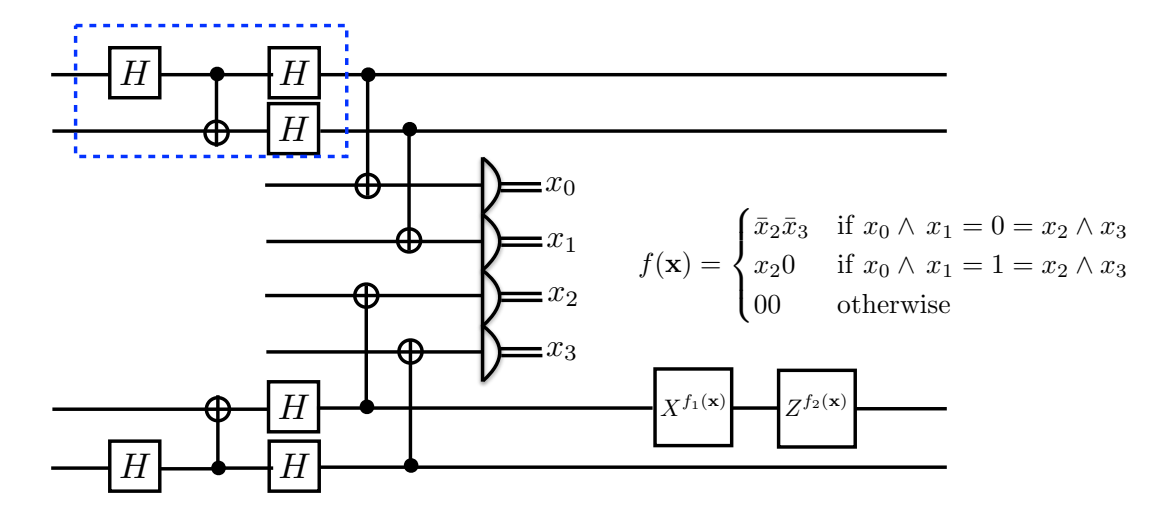


FIG. 10. A quantum circuit implementation for a pair of Hamiltonian anyons with M=2, d=2 prepared such that their global states belongs to $\mathcal{H}^{(\mathrm{Alt})}$. The top two qubits encode the energy spectrum of the particles whilst the bottom two the spin degrees of freedom. The subcircuit in blue performs a Bell basis measurement whose outcome is then imprinted onto the state of four auxiliary qubits (two for each Bell basis measurement). The outcome $x_0 = x_1 = 1$ (and likewise for x_2 and x_3) corresponds to the totally antisymmetric state. Depending on the measurement outcomes, $x_k \in \{0,1\}$, the function $f:\{0,1\}^4 \to \{0,1\}^2$, determines how the spin degrees of freedom are modified so that if the energy eigenstates are symmetric (antisymmetric) the corresponding spin states are antisymmetric (symmetric). The input states to the algorithm can be arbitrary, and the output states are then fed into an algorithm that prepares the thermal state for the Hamiltonian of Eq. (13).

VI. CONCLUSIONS

In this paper, we have introduced a novel model of statistical anyons. We have shown that the behavior of our model interpolates non-trivially between that of fermions and bosons. Our model exhibits rich thermodynamic properties, including phase transitions, that are controllable by external parameters. This dynamic behavior stands in sharp contrast to the more static properties of topological and statistical anyons, which lack such phase transitions. We have shown how Hamiltonian anyons can be controlled in order to construct engine cycles which exhibit enhancements in both their efficiency and power output as compared to a working medium of bosons, fermions, or statistical anyons. We have also demonstrated that Hamiltonian anyons can be simulated on NISQ quantum devices.

Our findings open several avenues for future research. While this study focuses on non-interacting particles, incorporating interactions could lead to even richer properties. In this initial approach, we penalized the space of nontrivial mixed symmetries, $\tilde{\mathcal{H}}$, to achieve a clear delineation of symmetric and antisymmetric subspaces. Including this space in our analysis might increase the complexity of the problem and reveal new physical phenomena.

In Ref. [50], it is shown that nontrivial parastatistics—distinct from both fermionic and bosonic statistics—can exist in physical systems. Extending our model to encompass this broader behavior would be an interesting extension. Lastly, an important direction for future work

is the simulation of anyons on real digital quantum computers, which are subject to noise and imperfections, presenting a key challenge. Investigating the effects of these factors on our model offers a valuable direction for future research.

ACKNOWLEDGMENTS

We thank Stefano Scali for advice on thermal state preparation in digital quantum computers. want to acknowledge funding from Ministry for Digital Transformation and of Civil Service of the Spanish Government through projects, PID2021-128970OA-I00 10.13039/501100011033 and QUANTUM ENIA project call - Quantum Spain project, and by the European Union through the Recovery, Transformation and Resilience Plan - NextGenerationEU within the framework of the Digital Spain 2026 Agenda, and also the FEDER/Junta de Andalucía program A.FQM.752.UGR20. JD acknowledges funding from the Engineering and Physical Sciences Research Council (EP/T518049/1). AT acknowledges funding from the Ministerio de Ciencia e Innovación of the Spanish Government through FPU20/02835. MS acknowledges support from the Ministerio de Ciencia e Innovación of the Spanish Government under the Ramón y Cajal funding scheme RYC2021-032032-I as well as FEDER funds C.EXP.256.UGR23 from the Junta de Andalucía. Finally, we are also grateful for the technical support provided by PROTEUS, the supercomputing center of the Institute Carlos I for Theoretical and Computational Physics in Granada, Spain.

- [1] A. Galindo and P. Pascual, *Quantum Mechanics* (Springer-Verlag, 1990).
- [2] A. Peres, Quantum Theory: concepts and methods (Kluwer Academic Publishers, 1995).
- [3] R. Bertlmann and N. Friis, Modern Quantum Theory: From Quantum Mechanics to Entanglement and Quantum Information (Oxford University Press, 2023).
- [4] W. Pauli, The Connection Between Spin and Statistics, Phys. Rev. 58, 716 (1940).
- [5] F. Wilczek, Quantum Mechanics of Fractional-Spin Particles, Phys. Rev. Lett. 49, 957 (1982).
- [6] F. Wilczek, From electronics to anyonics, Physics World 19, 22 (2006).
- [7] A. Stern, Anyons and the quantum Hall effect—A pedagogical review, Annals of Physics **323**, 204 (2008).
- [8] M. Carrega, L. Chirolli, S. Heun, and L. Sorba, Anyons in quantum Hall interferometry, Nat Rev Phys 3, 698–711 (2021).
- [9] A. Kitaev, Fault-tolerant quantum computation by anyons, Annals of Physics 303, 2 (2003).
- [10] V. Lahtinen and J. K. Pachos, A Short Introduction to Topological Quantum Computation, SciPost Phys. 3, 021 (2017).
- [11] J. Nakamura, S. Liang, G. C. Gardner, and M. J. Manfra, Direct Observation of Anyonic Braiding Statistics, Nature Physics 16, 931 (2020).
- [12] H. Bartolomei, M. Kumar, R. Bisognin, A. Marguerite, J.-M. Berroir, E. Bocquillon, B. Plaçais, A. Cavanna, Q. Dong, U. Gennser, Y. Jin, and G. Fève, Fractional statistics in anyon collisions, Science 368, 173 (2020).
- [13] M. Iqbal, N. Tantivasadakarn, R. Verresen, S. L. Campbell, J. M. Dreiling, C. Figgatt, J. P. Gaebler, J. Johansen, M. Mills, S. A. Moses, J. M. Pino, A. Ransford, M. Rowe, P. Siegfried, R. P. Stutz, M. Foss-Feig, A. Vishwanath, and H. Dreyer, Non-abelian topological order and anyons on a trapped-ion processor, Nature 626, 505 (2024).
- [14] S. Bose, Wärmegleichgewicht im Strahlungsfeld bei Anwesenheit von Materie, Zeitschrift für Physik 27, 384 (1924).
- [15] A. Einstein, Quantentheorie des einatomigen idealen Gases, Sitzungsberichte der Preussischen Akademie der Wissenschaften 22, 261 (1924).
- [16] P. A. M. Dirac, On the Theory of Quantum Mechanics, Proceedings of the Royal Society A 112, 661 (1926).
- [17] E. Fermi, Sulla quantizzazione del gas perfetto monoatomico, Rendiconti Lincei 3, 145–149 (1926).
- [18] L. Landau and E. Lifshitz, Statistical Physics (Mezhdunarodnaya Kniga, Moscow, 1988).
- [19] F. D. M. Haldane, Fractional statistics in arbitrary dimensions: A generalization of the Pauli principle, Phys. Rev. Lett. 67, 937 (1991).
- [20] Y.-S. Wu, Statistical distribution for generalized ideal gas of fractional-statistics particles, Phys. Rev. Lett. 73, 922 (1994).
- [21] M. V. N. Murthy and R. Shankar, Thermodynamics of a one-dimensional ideal gas with fractional exclusion statistics, Phys. Rev. Lett. 73, 3331 (1994).
- [22] N. M. Myers and S. Deffner, Thermodynamics of Statistical Anyons, PRX Quantum 2, 040312 (2021).
- [23] J. Gemmer, M. Michel, and G. Mahler, Quantum Ther-

- modynamics: Emergence of Thermodynamic Behavior Within Composite Quantum Systems (Springer Berlin, Heidelberg, 2009).
- [24] R. Kosloff, Quantum Thermodynamics: A Dynamical Viewpoint, Entropy 15, 2100 (2013).
- [25] S. Vinjanampathy and J. Anders, Quantum thermodynamics, Contemporary Physics 57, 545 (2016).
- [26] F. Binder, L. A. Correa, C. Gogolin, J. Anders, and G. Adesso, eds., Thermodynamics in the Quantum Regime: Fundamental Aspects and New Directions (Springer, 2018).
- [27] P. Strasberg, Quantum Stochastic Thermodynamics: Foundations and Selected Applications (Oxford University Press, 2022).
- [28] R. Alicki, The quantum open system as a model of the heat engine, Journal of Physics A: Mathematical and General 12, L103 (1979).
- [29] N. Linden, S. Popescu, and P. Skrzypczyk, How Small Can Thermal Machines Be? The Smallest Possible Refrigerator, Phys. Rev. Lett. 105, 130401 (2010).
- [30] M. O. Scully, K. R. Chapin, K. E. Dorfman, M. B. Kim, and A. Svidzinsky, Quantum heat engine power can be increased by noise-induced coherence, Proceedings of the National Academy of Sciences of the United States of America 108, 15097 (2011).
- [31] A. Tejero, D. Manzano, and P. I. Hurtado, Atom-doped photon engine: Extracting mechanical work from a quantum system via radiation pressure, Phys. Rev. E 109, 024141 (2024).
- [32] J. Klaers, S. Faelt, A. Imamoglu, and E. Togan, Squeezed thermal reservoirs as a resource for a nanomechanical engine beyond the carnot limit, Phys. Rev. X 7, 031044 (2017).
- [33] A. Tejero, D. Manzano, and P. I. Hurtado, Squeezing light to get non-classical work in quantum engines (2024), arXiv:2408.15085 [quant-ph].
- [34] N. M. Myers and S. Deffner, Bosons outperform fermions: The thermodynamic advantage of symmetry, Phys. Rev. E 101, 012110 (2020).
- [35] J. Koch, K. Menon, E. Cuestas, S. Barbosa, E. Lutz, T. Fogarty, T. Busch, and A. Widera, A quantum engine in the BEC–BCS crossover, Nature 621, 723 (2023).
- [36] J. B. Conway, A course in functional analysis (Springer, 2007)
- [37] L. Takhtadzhian, Quantum Mechanics for Mathematicians, Graduate Studies in Mathematics (American Mathematical Society, 2008).
- [38] K. Schönhammer, Thermodynamics and occupation numbers of a Fermi gas in the canonical ensemble, American Journal of Physics 68, 1032 (2000).
- [39] W. J. Mullin and J. P. Fernández, Bose–Einstein condensation, fluctuations, and recurrence relations in statistical mechanics, American Journal of Physics 71, 661 (2003).
- [40] R. Pathria and P. Beale, Statistical Mechanics (Academic Press, 2021).
- [41] P. Ehrenfest, Phasenumwandlungen im üblichen und erweiterten Sinn, classifiziert nach den entsprechenden Singularitäten des thermodynamischen Potentials, Verhandelingen der Koninklijke Akademie van Wetenschappen 36, 153 (1933).
- [42] D. Manzano and P. I. Hurtado, Symmetry and the ther-

modynamics of currents in open quantum systems, Phys. Rev. B **90**, 125138 (2014), publisher: American Physical Society.

- [43] D. Manzano and P. I. Hurtado, Harnessing symmetry to control quantum transport, Adv. Phys **67**, 1 (2018).
- [44] C. K. Hong, Z. Y. Ou, and L. Mandel, Measurement of subpicosecond time intervals between two photons by interference, Phys. Rev. Lett. 59, 2044 (1987).
- [45] Y. Zheng, P. Hänggi, and D. Poletti, Occurrence of discontinuities in the performance of finite-time quantum otto cycles, Phys. Rev. E 94, 012137 (2016).
- [46] J. Son, P. Talkner, and J. Thingna, Monitoring quantum otto engines, PRX Quantum 2, 040328 (2021).
- [47] K. Temme, T. J. Osborne, K. G. Vollbrecht, D. Poulin, and F. Verstraete, Quantum Metropolis sampling, Nature 471, 87 (2011).
- [48] C.-F. Chen, M. J. Kastoryano, F. G. S. L. Brandão, and A. Gilyén, Quantum thermal state preparation (2023), arXiv:2303.18224 [quant-ph].
- [49] The mixing time of any open system dynamics is defined as the time it takes for any pair of initial states to become indistinguishable.
- [50] Z. Wang and K. R. A. Hazzard, Particle Exchange Statistics beyond Fermions and Bosons, Nature 637, 314 (2025).
- [51] J.-P. Serre, Linear representations of finite groups (Springer, 1977).
- [52] R. Bishop and S. Goldberg, Tensor Analysis on Manifolds (Dover Publications, 1980).
- [53] W. Fulton and J. Harris, Representation Theory: A First Course (Springer, 1991).
- [54] S. Gustafson and I. Sigal, Mathematical concepts of quantum mechanics (Springer, 2003).
- [55] R. Goodman and N. R. Wallach, Symmetry, representations, and invariants (Springer, 2009).
- [56] B. C. Hall, Quantum theory for mathematicians (Springer, 2013).
- [57] B. C. Hall, Lie groups, Lie algebras, and representations (Springer, 2013).
- [58] P. Woit, Quantum theory, groups and representations (Springer, 2017).
- [59] I. Schur, Über eine Klasse von Matrizen, die sich einer gegebenen Matrix zuordnen lassen (Dieterich, 1901).
- [60] I. Schur, Über die rationalen Darstellungen der allgemeinen linearen Gruppe, Sitzungsberichte Akad. Berlin 1927, 58 (1927).
- [61] H. Weyl, The classical groups: their invariants and representations (Princeton University Press, 1939).
- [62] M. Fanizza, M. Skotiniotis, J. Calsamiglia, R. Muñoz-Tapia, and G. Sentís, Universal Algorithms for Quantum Data Learning, EPL 140, 28001 (2022).
- [63] The determination of the dimension of the spaces and their bases is a straightforward derivation in elementary tensor algebra. Here we show that the same result can be derived from a purely representation theory approach.

Appendix A: Hilbert spaces for the N anyons system

1. Representation theory and Schur-Weyl Duality

The following references provide all the information regarding the results presented in this section: [37, 51–58]. For simplicity and brevity, the proofs are omitted but can be found in the referenced sources. Note that, in this first subsection, we shall adopt \mathbb{C}^d in place of a generic d-dimensional complex vector space V without loss of generality, consistent with the notation of [55].

a. Representations of S_N

The most straightforward manner to compute and catalogue the irreducible representations of the permutation group of N elements, S_N , is by means of the so-called Young tableaux. This pictorial approach organizes the irreducible representations based on their behavior under permutations of two or more indices. The application to quantum mechanics becomes straightforward, enabling the distinction between symmetric spaces, antisymmetric spaces, and spaces with non-trivial symmetries.

Definition 1 (Ordered, integer partitions) An ordered, integer partition, λ , of $N \in \mathbb{Z}^+$, is a k-tuple $\lambda = (\lambda_1, \lambda_2, \dots, \lambda_k)$, such that $\lambda_1 \geq \lambda_2 \geq \dots \geq \lambda_k$, $\lambda_j \in \mathbb{Z}^+$ for all $1 \leq j \leq k$, satisfying

$$\sum_{i=1}^{k} \lambda_i = N. \tag{A1}$$

There exists a particularly useful method of representing ordered integer partitions that allows for easy computation of their corresponding irreducible representations. The following two definitions introduce this representation known as *Young diagrams* and *Young tableaux*.

Definition 2 (Young diagram) Let λ be an integer partition of N. A Young diagram corresponding λ is an arrangement of N boxes into k rows such that the number of boxes in row $i \in \{1, ..., r\}$ is equal to $\lambda_i \in \lambda$.

Definition 3 (Young Tableau) A Young tableau is a labeling of a Young diagram with the integers $(1, \ldots, N)$. A canonical, or standard, Young tableau is one where the labeling is increasing from left to right, and from top to bottom.

The permutation group of N elements, S_N , acts naturally on any Young tableau by permuting its labels, providing a framework for representing the irreducible representations of S_N . Consider a Young tableau corresponding to the partition λ of N, and define the following subgroups of S_N

$$P_{\lambda} := \{ \sigma \in S_N : \sigma \text{ preserves each row of } \lambda \},$$

 $Q_{\lambda} := \{ \tau \in S_N : \tau \text{ preserves each column of } \lambda \}.$ (A2)

To each of these two subgroups, the following two elements can be associated

$$A_{\lambda} = \sum_{\sigma \in P_{\lambda}} \sigma,$$

$$B_{\lambda} = \sum_{\tau \in Q_{\lambda}} \operatorname{sgn}(\tau)\tau,$$
(A3)

belonging to the group algebra of S_N —the complex vector space, $\mathbb{C}[S_N]$, with basis elements indexed by S_N . These elements enable the definition of the following construct.

Definition 4 (Young Symmetrizer) The Young symmetrizer of the partition λ , C_{λ} , is the element of the associated group algebra $\mathbb{C}[S_N]$ defined as

$$C_{\lambda} := A_{\lambda} B_{\lambda}. \tag{A4}$$

The action of S_N on N copies of any d-dimensional complex vector space \mathbb{C}^d , $\bigotimes^N \mathbb{C}^d$, by way of permuting its indices, allows to define a natural group algebra representation $\mathbb{C}[S_N] \to \operatorname{End}\left(\bigotimes^N \mathbb{C}^d\right)$. As we are interested in the symmetric and antisymmetric subspaces, the images of $A_\lambda, B_\lambda \subset \mathbb{C}[S_N]$ into $\bigotimes^N \mathbb{C}^d$ are

$$\operatorname{Im} A_{\lambda} = \operatorname{Sym}^{\lambda_{1}} \mathbb{C}^{d} \otimes \ldots \otimes \operatorname{Sym}^{\lambda_{k}} \mathbb{C}^{d} \subset \bigotimes^{N} \mathbb{C}^{d},$$

$$\operatorname{Im} B_{\lambda} = \operatorname{Alt}^{\lambda_{1}} \mathbb{C}^{d} \otimes \ldots \otimes \operatorname{Alt}^{\lambda_{k}} \mathbb{C}^{d} \subset \bigotimes^{N} \mathbb{C}^{d},$$
(A5)

respectively, where $\operatorname{Sym}^m \mathbb{C}^d$ is the totally symmetric subspace of $\bigotimes^m \mathbb{C}^d$, and $\operatorname{Alt}^m \mathbb{C}^d$ is the totally antisymmetric subspace of $\bigotimes^m \mathbb{C}^d$, for $m \in \{\lambda_1, \ldots, \lambda_k\}$. The following theorem then establishes a connection between the Young symmetrizer and the irreducible representations of S_N [53, 55].

Theorem 1 The image of the Young symmetrizer C_{λ} in $\mathbb{C}[S_N]$

$$Im C_{\lambda} = \mathbb{C}[S_N]C_{\lambda} \equiv \mathcal{V}_{\lambda}, \tag{A6}$$

is an irreducible representation of the group S_N . Every irreducible representation of S_N is isomorphic to \mathcal{V}_{λ} for some partition λ .

The irreducible representation V_{λ} is referred to as a Specht module.

By way of example, consider the Young tableaux consisting of a single row, $\lambda = (d)$, and a single column $\lambda = (1, 1, ..., 1) := (\mathbf{1})$. For $\lambda = (d)$, $P_{(d)} = S_N$ and $Q_{(d)} = \{1\}$ so that

$$C_{(d)} = A_{(d)} = \sum_{\sigma \in S_N} \sigma, \tag{A7}$$

which implies that the image of $C_{(d)}$ on the vector space $\bigotimes^N \mathbb{C}^d$ is $\operatorname{Sym}^d \mathbb{C}^d$ —the totally symmetric subspace of

 $\bigotimes^N \mathbb{C}^d.$ Similarly, for $\lambda=(\mathbf{1})$, $P_{(\mathbf{1})}=\{1\}$ and $Q_{(\mathbf{1})}=S_N$ so that

$$C_{(1)} = B_{(1)} = \sum_{\tau \in S_N} \text{sgn}(\tau)\tau,$$
 (A8)

meaning that the image of $C_{(1)}$ on $\bigotimes^N \mathbb{C}^d$ is $\operatorname{Alt}^d \mathbb{C}^d$ —the totally antisymmetric subspace of $\bigotimes^N \mathbb{C}^d$. The dimension of the irreducible representation \mathcal{V}_{λ} can be obtained via the Hook length formula

$$\dim \mathcal{V}_{\lambda} = \frac{N!}{\prod_{i,j} h(i,j)} := m_{\lambda}, \tag{A9}$$

where h(i, j) is the hook length of the box located in the ith row and j-th column given by

$$h(i,j) = (\lambda_i - j) + (\lambda'_i - i) + 1,$$
 (A10)

with λ'_j the number of boxes in the j-th column (equivalently the number of boxes in the j-th row of the transpose Young diagram corresponding to λ). For $\lambda = (\mathbf{1}), (N)$, dim $\mathcal{V}_{(\mathbf{1})} = \dim \mathcal{V}_{(N)} = 1$. This expression for the dimension of \mathcal{V}_{λ} allows us to determine the number of Young tableaux of a given Young diagram, i.e., m_{λ} provides the number of tableaux for a given λ .

b. Schur-Weyl duality

In addition to the action of S_N , the vector space $\bigotimes^N \mathbb{C}^d$ naturally carries the action of $\mathrm{GL}(d,\mathbb{C})$. This is particularly relevant when $\bigotimes^N \mathbb{C}^d$ corresponds to the state space of N identical particles with a d-valued degree of freedom. This result by Schur and Weyl [59–61] establishes a connection between the irreducible components of S_N and those of $\mathrm{GL}(d,\mathbb{C})$, enabling the determination of the collective behavior of the degrees of freedom of particles associated with $\mathrm{GL}(d,\mathbb{C})$ under particle exchange [62].

Specifically, for all integers $d \geq 0$, let $\pi : \operatorname{GL}(d, \mathbb{C}) \to \bigotimes^N \mathbb{C}^d$, and $T : S_N \to \bigotimes^N \mathbb{C}^d$ be representations of $\operatorname{GL}(d, \mathbb{C})$ and S_N respectively whose action on $\bigotimes^N \mathbb{C}^d$ is defined as

$$\pi(g)(v_1 \otimes \ldots \otimes v_d) = g(v_1) \otimes \ldots \otimes g(v_N),$$

$$T(\sigma)(v_1 \otimes \ldots \otimes v_d) = v_{\sigma^{-1}(1)} \otimes \ldots \otimes v_{\sigma^{-1}(N)},$$
(A11)

for $g \in GL(d, \mathbb{C}), \sigma \in S_N$, where $v_i \in \mathbb{C}^d$, for $i = 1, \ldots, N$. As it is possible to permute the factors without changing the action of $GL(d, \mathbb{C})$, the actions of these two groups commute. In fact, the spans of the images of $GL(d, \mathbb{C})$ and S_N in End $(\bigotimes^N \mathbb{C}^d)$ act as double centralizers. This result establishes a profound connection between the representations of these two groups (for a more detailed discussion about mutual centralizers, see [55]). To elucidate on this relation we require the following definition.

Definition 5 (Schur functor) The Schur functor \mathbb{S}_{λ} of a partition λ is the image of the Young symmetrizer C_{λ} on $\bigotimes^{N} \mathbb{C}^{d}$. Moreover, $\mathbb{S}_{\lambda}\mathbb{C}^{d}$ is a representation of $\mathrm{GL}(\mathrm{N},\mathbb{C})$.

The Schur functor satisfies the following properties. Let $U, V, W \in \mathbb{C}^d$, and let $f: V \to W, g: U \to V$ be linear maps. Then $\mathbb{S}_{\lambda} f: \mathbb{S}_{\lambda} V \to \mathbb{S}_{\lambda} W$ such that for any $\Psi \in \mathbb{S}_{\lambda} V$ it holds

$$\mathbb{S}_{\lambda} f(\Psi) = f^{\otimes N} \circ \Psi \in \mathbb{S}_{\lambda} W. \tag{A12}$$

Moreover, $\mathbb{S}_{\lambda}(f \circ g) = \mathbb{S}_{\lambda} f \circ \mathbb{S}_{\lambda} g$ and $\mathbb{S}_{\lambda}(\mathrm{Id}_{V}) = \mathrm{Id}_{\mathbb{S}_{\lambda}}$. With this, we can now state the content of Schur-Weyl duality.

Theorem 2 (Schur-Weyl duality) The decomposition

$$\bigotimes^{N} \mathbb{C}^{d} \cong \bigoplus_{\lambda} \mathcal{V}_{\lambda} \otimes \mathbb{S}_{\lambda} \mathbb{C}^{d}$$
 (A13)

is a representation of $S_N \times \operatorname{GL}(d,\mathbb{C})$. Here, \mathcal{V}_{λ} ranges over all irreducible representations of S_N , Eq. (A6), and each $\mathbb{S}_{\lambda}\mathbb{C}^d$ is either an irreducible representation of $\operatorname{GL}(d,\mathbb{C})$ or zero. $\mathbb{S}_{\lambda}\mathbb{C}^d=0$ if the partition of N has more than d parts, i.e., $\lambda > \dim \mathbb{C}^d$.

The proof of the Schur-Weyl theorem relies on the result stated in the *double centralizer theorem*, see [55]. See also Theorem 6.3, and Lemmas 6.22–6.23 in [53] for the proof.

As an example, consider the totally symmetric and antisymmetric subspaces, corresponding to the partitions $\lambda = (N), \lambda = (1)$, of the space $\bigotimes^N \mathbb{C}^d$. The Schur functors $\mathbb{S}_{(N)}\mathbb{C}^d$ and $\mathbb{S}_{(1)}\mathbb{C}^d$ correspond to $\operatorname{Sym}^N \mathbb{C}^d$ and $\operatorname{Alt}^N \mathbb{C}^d$ respectively. Note that $\operatorname{Alt}^N \mathbb{C}^d$ vanishes if $\dim \mathbb{C}^d < N$. According to Schur-Weyl duality, stated in Theorem 2, we can write the following representation of $\operatorname{GL}(N,\mathbb{C})$

$$\bigotimes^{N} \mathbb{C}^{d} \cong \bigoplus_{\lambda} \left(\mathbb{S}_{\lambda} \mathbb{C}^{d} \right)^{\oplus m_{\lambda}}, \tag{A14}$$

and the irreducible representations of $\mathrm{GL}(N,\mathbb{C})$ can be obtained directly from those of S_N . For instance, for N=2, Eq. (A14) reduces to

$$\mathbb{C}^d \otimes \mathbb{C}^d \cong \operatorname{Sym}^2 \mathbb{C}^d \oplus \operatorname{Alt}^2 \mathbb{C}^d, \tag{A15}$$

which is the canonical decomposition of a product of two vector spaces into their symmetric and antisymmetric parts. For N=3,4, Eq. (A14) reads

$$\bigotimes_{k=1}^{3} \mathbb{C}_{k}^{d} \cong \operatorname{Sym}^{3} \mathbb{C}^{d} \oplus \left(\mathbb{S}_{(2,1)} \mathbb{C}^{d} \right)^{\oplus 2} \oplus \operatorname{Alt}^{3} \mathbb{C}^{d}, \quad (A16)$$



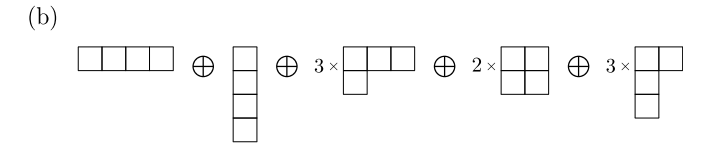


FIG. 11. Diagrammatic representations of the (a) N=3 decomposition, see Eq. (A16), and (b) N=4 decomposition, see Eq. (A17).

$$\bigotimes_{k=1}^{4} \mathbb{C}_{k}^{d} \cong \operatorname{Sym}^{4} \mathbb{C}^{d} \oplus \operatorname{Alt}^{4} \mathbb{C}^{d}$$

$$\oplus (\mathbb{S}_{(3,1)} \mathbb{C}^{d})^{\oplus 3} \oplus (\mathbb{S}_{(2,2)} \mathbb{C}^{d})^{\oplus 2} \oplus (\mathbb{S}_{(2,1,1)} \mathbb{C}^{d})^{\oplus 3}.$$
(A17)

The non-trivial irreducible representation $\mathbb{S}_{(2,1)}\mathbb{C}^d$ appears twice for the case of N=3, whilst the non-trivial irreducible representations $\mathbb{S}_{(3,1)}\mathbb{C}^d$, $\mathbb{S}_{(2,2)}\mathbb{C}^d$, and $\mathbb{S}_{(2,1,1)}\mathbb{C}^d$ appear three times, twice, and three times respectively for the case of N=4. The diagrammatic representation of these examples is depicted in Fig. 11. As we will be solely interested in the totally symmetric and antisymmetric representations of S_N , we can write Eq. (A14) as

$$\bigotimes^{N} \mathbb{C}^{d} \cong \operatorname{Sym}^{N} \mathbb{C}^{d} \oplus \operatorname{Alt}^{N} \mathbb{C}^{d} \oplus \mathscr{V}(\text{other}), \quad (A18)$$

where $\mathcal{V}(\text{other})$ accounts for all other *exotic* symmetries that may appear in the decomposition.

We conclude this section by computing the dimension of the vector spaces corresponding to the symmetric and antisymmetric subspaces of $\bigotimes^N \mathbb{C}^d$, as well as providing an orthonormal basis for each one.

Proposition 1 Let λ be a tableau of dimension N and $\dim \mathbb{C}^d = d$. The dimension of the Schur functor $\mathbb{S}_{\lambda}\mathbb{C}^d$

$$\dim \mathbb{S}_{\lambda} \mathbb{C}^{d} = \prod_{i,j} \frac{\lambda_{i} - \lambda_{j} + j - i}{j - i} = \frac{m_{\lambda}}{N!} \prod_{i,j} (d - i + j),$$
(A19)

where the products are over the pairs (i, j) that label the row and column of λ respectively.

Analyzing the completely symmetric and antisymmetric cases, $m_{(N)} = m_{(1)} = 1$, as they are the only irreducible representations of the corresponding tableau. Then, the dimension of the symmetric and antisymmetric subspaces are directly obtained by computing the dimension of the

Schur functor for these tableaux, i.e.,

$$\dim \mathbb{S}_{(N)} \mathbb{C}^{d} = \frac{\prod_{i=1,j=1,\dots,N} (d-i+j)}{N!},$$

$$= \binom{d+N-1}{N}$$

$$\dim \mathbb{S}_{(1)} \mathbb{C}^{d} = \frac{\prod_{i=1,\dots,N,j=1} (d-i+j)}{N!}$$

$$= \binom{d}{N}.$$
(A20)

A basis for these spaces can be constructed using the following proposition [52].

Proposition 2 Let $\{e_i\}_{i=1}^d$ a basis of \mathbb{C}^d . For the totally symmetric and antisymmetric subspaces, we can construct the following orthogonal basis

$$B_{\operatorname{Sym}^{N} \mathbb{C}^{d}} = \left\{ \sum_{\sigma \in S_{N}} e_{\sigma(1)} \otimes \ldots \otimes e_{\sigma(N)} \right\},$$

$$B_{\operatorname{Alt}^{N} \mathbb{C}^{d}} = \left\{ \sum_{\tau \in S_{N}} \operatorname{sgn}(\tau) e_{\tau(1)} \otimes \ldots \otimes e_{\tau(N)} \right\}.$$
(A21)

In the context of quantum mechanics, the dimensions of these spaces are directly related to the degrees of freedom available to N identical particles with d internal states. For bosonic systems (totally symmetric), $\dim \mathbb{S}_{(N)}\mathbb{C}^d$ corresponds to the number of possible configurations of N bosons occupying d states. In the case of fermionic systems (totally antisymmetric), $\dim \mathbb{S}_{(1)}\mathbb{C}^d$ represents the number of possible configurations for N fermions obeying the Pauli exclusion principle [63].

2. Hilbert spaces

Consider a quantum particle with spin j. In general, the total Hilbert space describing it has two terms

$$\mathcal{H} = \mathscr{H} \otimes V_d, \tag{A22}$$

where \mathscr{H} is the space related to the internal degrees of freedom, e.g. the position of the particle, and V_d is a complex vector space of dimension d, with d=2j+1, carrying an irreducible representation of $\mathrm{SU}(d)$. It is convenient to represent the total state of the system $|\Psi\rangle \in \mathcal{H}$ can be written as $\Psi = \psi(r)\chi(s)$, where $\psi(r) \in \mathscr{H}$, for $r \in \mathbb{R}^3$, and $\chi(s) \in V_d$. This variable s depends on the spin of the particle, and takes the 2j+1 values from $\{-j,-j+1,\ldots,j+1,j\}$. The vector space V_d is isomorphic to the complex numbers so that $V_d \cong \mathbb{C}^d = \mathbb{C}^{2j+1}$. Note that we are abusing the notation when writing $\chi(s)$. What we are really doing is identifying the complex space \mathbb{C}^{2j+1} with the space of functions

$$\chi: \{-j, -j+1, \dots, j-1, j\} \longrightarrow \mathbb{C}, \tag{A23}$$

so that, for every element $e_i \in B_{\mathbb{C}^{2j+1}} = \{e_1, \dots, e_{2j+1}\},$ we assign the function χ_i acting as

$$\chi_i(j+1-i) = 1; \text{ 0 otherwise,} \tag{A24}$$

for all i = 1, ..., 2j + 1. This identification generalizes the concept of spinor to particles with any arbitrary spin, see [37] for further details.

Consider a quantum system composed of N identical particles with spin j. The total Hilbert space corresponding to the total system is N times the individual one, Eq. (A22), namely

$$\mathcal{H}^{\otimes N} = \mathcal{H}^{\otimes N} \otimes V_J^{\otimes N}. \tag{A25}$$

As stated in Eq. (A11), there is a natural action of the permutation group of N elements, S_N , on the total Hilbert space given by Eq. (A25). Consider the general N-particle Hamiltonian acting on the system

$$H_N = -\frac{\hbar}{2m} \sum_{i=1}^{N} p_i^2 + \sum_{i=1}^{N} \phi_{\text{int}}(\boldsymbol{r}_i) + \sum_{i < j} \phi_{\text{ext}}(\boldsymbol{r}_i - \boldsymbol{r}_j),$$
(A26)

where m is the mass of the particles, which has been assumed to be equal for all of them without loss of generality. Then, by virtue of this natural action of the permutation group, $[H_N, T_N(\sigma)] = 0$, for any given $\sigma \in S_N$, and any representation T_N of S_N on the total Hilbert space. The direct consequence of this result dictates that H_N can be restricted to invariant subspaces of $\mathcal{H}^{\otimes N}$, and particularly to $\mathcal{H}^{(\mathrm{Sym})}$ and $\mathcal{H}^{(\mathrm{Alt})}$. That is, for bosonic particles, the Hilbert space for N-particle systems is the totally symmetric subspace $\mathcal{H}^{(\mathrm{Sym})}$ of the N-fold product in Eq. (A25). The same applies for fermions with the totally antisymmetric subspace $\mathcal{H}^{(\mathrm{Alt})}$. Note that the total Hamiltonian, Eq. (A26), does not act on the spin variables.

As a consequence of the Schur-Weyl duality, Eqs. (A13)-(A18), the total Hilbert $\mathcal{H}^{\otimes N}$ space decomposes into a direct sum of irreducible subspaces $\mathcal{H}^{(\lambda)}$, that correspond to the different symmetries of the N particles under permutations. This means that the irreducible representations of S_N are connected to the ones of $\mathrm{SU}(d)$ which are carried by the spaces V_d , allowing us to elucidate the total spin of the corresponding wavefunctions. Then,

$$\mathcal{H}^{\otimes N} \cong \bigoplus_{\lambda} \mathcal{H}^{(\lambda)},$$
 (A27)

where the terms $\mathcal{H}^{(\lambda)}$ are the subspaces carrying the irreducible representations of S_N labeled by λ . The totally symmetric and antisymmetric subspaces decompose as

$$\mathcal{H}^{(\mathrm{Sym})} = \left[\mathscr{H}^{\otimes N} \right]^{(\mathrm{Sym})} \otimes \left[V_d^{\otimes N} \right]^{(\mathrm{Sym})}$$

$$\oplus \left[\mathscr{H}^{\otimes N} \right]^{(\mathrm{Alt})} \otimes \left[V_d^{\otimes N} \right]^{(\mathrm{Alt})}$$

$$\oplus \tilde{\mathcal{H}}^{(\mathrm{Sym})}, \tag{A28}$$

$$\mathcal{H}^{(\mathrm{Alt})} = \left[\mathscr{H}^{\otimes N} \right]^{(\mathrm{Sym})} \otimes \left[V_d^{\otimes N} \right]^{(\mathrm{Alt})}$$

$$\oplus \left[\mathscr{H}^{\otimes N} \right]^{(\mathrm{Alt})} \otimes \left[V_d^{\otimes N} \right]^{(\mathrm{Sym})}$$

$$\oplus \tilde{\mathcal{H}}^{(\mathrm{Alt})}$$
(A29)

where $\tilde{\mathcal{H}}^{(\mathrm{Sym})}$, $\tilde{\mathcal{H}}^{(\mathrm{Alt})}$ correspond to the product spaces of non-trivial symmetries which, when multiplied, give rise to totally symmetric and antisymmetric spaces respectively. In the particular case of two particles with spin 1/2, the total Hilbert space is directly

$$\mathcal{H}^{\otimes 2} = \mathcal{H}^{\otimes 2} \otimes V_2^{\otimes 2}. \tag{A30}$$

Since the system consists of two fermions, we are interested in the totally antisymmetric subspace, which, from Eq. (A29), decomposes as

$$\mathcal{H}^{(\mathrm{Alt})} = \left[\mathscr{H}^{\otimes 2} \right]^{(\mathrm{Sym})} \otimes \left[V_2^{\otimes 2} \right]^{(\mathrm{Alt})}$$

$$\oplus \left[\mathscr{H}^{\otimes 2} \right]^{(\mathrm{Alt})} \otimes \left[V_2^{\otimes 2} \right]^{(\mathrm{Sym})},$$
(A31)

where $V_2^{\otimes 2} \cong \mathbb{C}^2 \otimes \mathbb{C}^2$. Using the general expressions for the basis in the totally symmetric and antisymmetric spaces in Proposition 2, the basis for this particular case are

$$\operatorname{Sym}^{2} \mathbb{C}^{2} = \operatorname{span} \left\{ e_{1} \otimes e_{1}, e_{1} \otimes e_{2} + e_{2} \otimes e_{1}, e_{2} \otimes e_{2} \right\},$$
(A32)

$$\operatorname{Alt}^{2} \mathbb{C}^{2} = \operatorname{span} \left\{ e_{1} \otimes e_{2} - e_{2} \otimes e_{1} \right\}, \tag{A33}$$

where $\{e_1, e_2\}$ is a basis of \mathbb{C}^2 . This particular case is straightforward to compute and can be directly derived from the irreducible representations of SU(2) using the Clebsch-Gordan decomposition. Let us label the vector space V by the value of the associated spin, j and j'. The product of two spaces V_j and $V_{j'}$ is then decomposed as

$$V_j \otimes V_{j'} = \bigoplus_{l=|j-j'|}^{|j+j'|} V_l. \tag{A34}$$

In our specific case, where j = j' = 1/2, this results in

$$V_{1/2} \otimes V_{1/2} = V_0 \oplus V_1.$$
 (A35)

The basis for V_0 can be computed directly, yielding the state in Eq. (A33), while the basis for V_1 corresponds to the state in Eq. (A32). The dimension for V_0 is one, and for V_1 is three, directly derived from the relation between the dimension and spin, l=2j+1. This is the reason why in physics terminology one refers to the antisymmetric space as singlet, and to the symmetric one as triplet. For more details, consult [57, 58]. Although the Clebsch-Gordan decomposition is manageable for two particles, it becomes increasingly complex when applied to products involving more terms. For systems with more than a few particles, the use of Schur-Weyl duality becomes essential to handle the computations effectively.

Appendix B: Calculations of thermodynamic quantities

In this appendix, we expand on some of the calculations presented in Sec. III, concerning the thermal properties of Hamiltonian anyons in a harmonic potential. For completeness, we first note that the N-particle, noninteracting, one-dimensional harmonic oscillator Hamiltonian is explicitly given (before symmetrization) by

$$H_{\rm HO} = \bigoplus_{k=1}^{N} \left[\sum_{n_k=0}^{\infty} \hbar \omega \left(n_k + \frac{1}{2} \right) |n_k\rangle \langle n_k| \right], \qquad (B1)$$

where $|n_k\rangle$ denotes the state where the k-th particle occupies the $n^{\rm th}$ energy level. The task of computing the canonical partition function for bosons or fermions with this Hamiltonian is nontrivial, but can be achieved by using the grand canonical ensemble to obtain a recursion relation for successive numbers of particles, N. See Ref. [39] for more details.

To obtain the reduced thermal state of the harmonic oscillator degrees of freedom, we proceed from Eq. (15)

$$\tau_{\mathscr{H}^{\otimes N}} = \operatorname{Tr}_{(\mathbb{C}^{d})^{\otimes N}} \left\{ \left[\frac{1}{Z} e^{-\beta H} \right]^{(\operatorname{Alt})} \right\} \\
= \frac{1}{Z} \left[e^{-\beta H_{\operatorname{HO}}} \right]^{(\operatorname{Alt})} \operatorname{Tr} \left[\Pi_{(\mathbb{C}^{d})^{\otimes N}}^{(\operatorname{Sym})} \right] \\
+ \frac{1}{Z} e^{-\beta \nu} \left[e^{-\beta H_{\operatorname{HO}}} \right]^{(\operatorname{Sym})} \operatorname{Tr} \left[\Pi_{(\mathbb{C}^{d})^{\otimes N}}^{(\operatorname{Alt})} \right] \\
= \binom{d+N-1}{N} \frac{Z_{\operatorname{F}}}{Z} \left(\frac{1}{Z_{\operatorname{F}}} \left[e^{-\beta H_{\operatorname{HO}}} \right]^{(\operatorname{Alt})} \right) \\
+ \binom{d}{N} e^{-\beta \nu} \frac{Z_{\operatorname{B}}}{Z} \left(\frac{1}{Z_{\operatorname{B}}} \left[e^{-\beta H_{\operatorname{HO}}} \right]^{(\operatorname{Sym})} \right) \\
= \binom{d+N-1}{N} \frac{Z_{\operatorname{F}}}{Z} \tau_{\operatorname{F}} + \binom{d}{N} e^{-\beta \nu} \frac{Z_{\operatorname{B}}}{Z} \tau_{\operatorname{B}}, \\
\end{cases}$$
(B2)

where the fermionic/bosonic thermal states are $\tau_{\rm F/B} = \frac{1}{Z_{\rm F/B}} \left[e^{-\beta H_{\rm HO}} \right]^{\rm (Alt/Sym)}$. The binomial factors appear directly when tracing out the projectors $\Pi_{(\mathbb{C}^d)^{\otimes N}}^{\rm (Sym/Alt)}$, providing the dimension of the symmetric/antisymmetric auxiliary subspaces as in Eq. (A20).

We define $p_{\rm F}$ as the prefactor on $\tau_{\rm F}$

$$p_{\rm F} = {d+N-1 \choose N} \frac{Z_{\rm F}}{Z} = \frac{{d+N-1 \choose N} Z_{\rm F}}{{d+N-1 \choose N} Z_{\rm F} + {d \choose N} e^{-\beta \nu} Z_B}.$$
(B3)

Note that, from Eq. (17), $\frac{Z_B}{Z_F} = e^{\frac{1}{2}\beta\hbar\omega(N^2-N)}$. Let us define $h(d,N) := \ln\binom{d+N-1}{N} - \ln\binom{d}{N}$. Then, p_F can be trivially expressed as in Eq. (19).

The internal energy can be computed from the parti-

tion function as follows

$$\begin{split} U &= -\frac{1}{Z} \frac{\partial Z}{\partial \beta} \\ &= -\frac{1}{Z} \left[\binom{d+N-1}{N} \frac{\partial Z_{\rm F}}{\partial \beta} + \binom{d}{N} \frac{\partial}{\partial \beta} \left(e^{-\beta \nu} Z_{\rm B} \right) \right] \\ &= \binom{d+N-1}{N} \frac{Z_{\rm F}}{Z} U_{\rm F} + \binom{d}{N} e^{-\beta \nu} \frac{Z_{\rm B}}{Z} (\nu + U_{\rm B}) \\ &= p_{\rm F} U_{\rm F} + (1-p_{\rm F})(\nu + U_{\rm B}), \end{split} \tag{B4}$$

where the fermionic and bosonic internal energies can be straightforwardly calculated from Eq. (17) using that $U_{\rm F/B} = -\frac{\partial}{\partial \beta} \ln Z_{\rm F/B}$.

Appendix C: Capacities and Phase Transitions

In this appendix, we compute the first and second derivatives of the internal energy for N Hamiltonian anyons, Eq. (B4), to identify first- and second-order phase transitions. The first derivative, which corresponds to the heat capacity with respect to each of the parameters $X \in \{T, \nu, \omega\}$ of the system are given by

$$C_{X} \equiv \frac{\partial U}{\partial X} = p_{F} \left(\frac{\partial U_{F}}{\partial X} - \frac{\partial U_{B}}{\partial X} - \frac{\partial \nu}{\partial X} \right) + \frac{\partial U_{B}}{\partial X} + \frac{\partial \nu}{\partial X}$$

$$+ \frac{\partial p_{F}}{\partial X} (U_{F} - U_{B} - \nu)$$

$$= p_{F} \left(\frac{\partial U_{F}}{\partial X} - \frac{\partial U_{B}}{\partial X} - \frac{\partial \nu}{\partial X} \right) + \frac{\partial U_{B}}{\partial X} + \frac{\partial \nu}{\partial X}$$

$$- p_{F}^{2} \left(\frac{\partial \phi}{\partial X} \right) e^{\phi} (U_{F} - U_{B} - \nu) ,$$
(C1)

where the parameter ϕ reads

$$\phi = \frac{\hbar \omega \beta}{2} N(N-1) - \nu \beta - h(d, N).$$
 (C2)

To derive Eq. (C1), it is convenient to make use of the following identity for $p_{\rm F}$

$$\frac{\partial p_{\rm F}}{\partial X} = \frac{\partial}{\partial X} \left(\frac{1}{1 + e^{\phi}} \right) = -p_{\rm F}^2 \left(\frac{\partial \phi}{\partial X} \right) e^{\phi}. \tag{C3}$$

Noting that neither $U_{\rm B}$ nor $U_{\rm F}$ depend explicitly on ν , i.e.,

$$\frac{\partial U_{\rm B}}{\partial \nu} = \frac{\partial U_{\rm F}}{\partial \nu} = 0, \tag{C4}$$

and that their derivatives with respect to β and ω are, respectively

$$\frac{\partial U_{\rm B}}{\partial \beta} = \frac{\partial U_{\rm F}}{\partial \beta} = -\frac{\hbar^2 \omega^2}{4} \sum_{k=1}^N k^2 \operatorname{csch}^2\left(\frac{k\hbar\beta\omega}{2}\right),$$

$$\frac{\partial U_{\rm B}}{\partial \omega} = \frac{\hbar N}{2} - \hbar \sum_{k=1}^N \frac{k}{(1 - e^{k\beta\hbar\omega})^2}$$

$$-\frac{\hbar^2 \beta \omega}{4} \sum_{k=1}^N k^2 \operatorname{csch}^2\left(\frac{k\hbar\beta\omega}{2}\right),$$

$$\frac{\partial U_{\rm F}}{\partial \omega} = \frac{\hbar N^2}{2} - \hbar \sum_{k=1}^N \frac{k}{(1 - e^{k\beta\hbar\omega})^2}$$

$$-\frac{\hbar^2 \beta \omega}{4} \sum_{k=1}^N k^2 \operatorname{csch}^2\left(\frac{k\hbar\beta\omega}{2}\right).$$
(C5)

From these derivatives, we can compute the heat capacities, Eq. (C1)

$$\frac{\partial U}{\partial T} = k_{\rm B} \beta^2 \left\{ p_{\rm F}^2 e^{\phi} \left[\frac{\hbar \omega}{2} N(N-1) - \nu \right]^2 - \frac{\partial U_{\rm B}}{\partial \beta} \right\},
\frac{\partial U}{\partial \nu} = 1 - p_{\rm F} + p_{\rm F}^2 \beta e^{\phi} \left[\frac{\hbar \omega}{2} N(N-1) - \nu \right],
\frac{\partial U}{\partial \omega} = \frac{\hbar p_{\rm F}}{2} N(N-1) + \frac{\partial U_{\rm B}}{\partial \omega}
- \frac{\hbar \beta p_{\rm F}^2 e^{\phi}}{2} N(N-1) \left[\frac{\hbar \omega}{2} N(N-1) - \nu \right].$$
(C6)

Having computed the derivatives, we seek to identify non-analytical behavior for the heat capacities in the asymptotic limit of a large number of particles. Specifically, we are interested in the heat capacity per particle, but as we have mixtures of both bosons and fermions—with the latter obeying the Pauli exclusion principle—we search for non-analyticity of the following limit

$$\lim_{N \to \infty} \frac{1}{N^2} \frac{\partial U}{\partial X}.$$
 (C7)

Noting that the derivatives of the bosonic internal energies vanishes in this limit

$$\lim_{N \to \infty} \frac{1}{N^2} \frac{\partial U_{\rm B}}{\partial \beta} = 0$$

$$\lim_{N \to \infty} \frac{1}{N^2} \frac{\partial U_{\rm B}}{\partial \omega} = 0,$$
(C8)

the limits for the total internal energy with respect to the parameters $X \in \{T, \nu, \omega\}$, see Eq. (C1), are dominated by the fermionic behavior in the following form

$$\begin{split} &\lim_{N \to \infty} \frac{1}{N^2} \frac{\partial U}{\partial T} \\ &= k_{\rm B} \beta^2 \lim_{N \to \infty} \left\{ \frac{p_{\rm F}^2 e^\phi}{N^2} \left[\frac{\hbar \omega}{2} N(N-1) - \nu \right]^2 \right\}, \end{split}$$

$$\lim_{N \to \infty} \frac{1}{N^2} \frac{\partial U}{\partial \nu} = \lim_{N \to \infty} \left\{ \frac{\beta p_{\rm F}^2 e^{\phi}}{N^2} \left[\frac{\hbar \omega}{2} N(N-1) - \nu \right] \right\}, \tag{C9}$$

$$\begin{split} &\lim_{N \to \infty} \frac{1}{N^2} \frac{\partial U}{\partial \omega} \\ &= \frac{\hbar p_{\rm F}}{2} - \frac{\hbar \beta}{2} \lim_{N \to \infty} \left\{ \left[\frac{\hbar \omega}{2} N(N-1) - \nu \right] \right\}. \end{split}$$

Observe, however, that the parameters β, ν, ω are not independent as is evident from Eq. (C2). Importantly, note that $p_{\rm F}$ experiences a sharp transition around the value $\phi=0$, where its second derivative

$$\frac{\partial^2 p_{\rm F}}{\partial X^2} = p_{\rm F}^2 \left(\frac{\partial \phi}{\partial X}\right)^2 e^{\phi} \left(2p_{\rm F}e^{\phi} - 1\right),\tag{C10}$$

equals zero. Therefore, substituting

$$\nu = \frac{\hbar\omega}{2}N(N-1) - \frac{h(d,N)}{\beta} - \frac{\varepsilon}{\beta},$$
 (C11)

for $\varepsilon > 0$ into Eq. (C6), and taking the asymptotic limit,

we obtain the following behavior for the capacities

$$\begin{split} \lim_{N \to \infty} \frac{1}{N^2} \frac{\partial U}{\partial T} &= k_{\rm B} \beta^2 \lim_{N \to \infty} \left\{ \frac{p_{\rm F}^2 e^{\phi}}{\beta^2} \frac{[h(d,N) + \varepsilon]^2}{N^2} \right\} \\ &= \frac{k_{\rm B}}{4}, \end{split}$$

$$\lim_{N \to \infty} \frac{1}{N^2} \frac{\partial U}{\partial \nu} = p_{\rm F}^2 e^{\phi} \lim_{N \to \infty} \left\{ \frac{h(d, N) + \varepsilon}{N^2} \right\} = 0, \tag{C12}$$

$$\lim_{N \to \infty} \frac{1}{N^2} \frac{\partial U}{\partial \omega} = \frac{\hbar p_{\rm F}}{2} - \frac{\hbar}{2} \lim_{N \to \infty} \{h(d, N) + \varepsilon\} = -\infty.$$

Note that, in the thermodynamic limit $(N \to \infty)$, the function h(d, N) tends to

$$h(d, N) \to \begin{cases} \log \frac{N}{d} & \text{for } d \gg N, \\ 2N & \text{for } d = N. \end{cases}$$
 (C13)

The divergence in the capacity with respect to ω occurs due to the fact that the ground state energy for Hamiltonian anyons jumps from linear to quadratic in the number of particles as ω approaches the value for which $\phi=0$. This can be clearly seen in Fig. 2(b), where the spread of the phase transition with respect to each of the three parameters is also illustrated. Finally, the second-order derivative of the internal energy is

$$\frac{\partial^{2} U}{\partial X^{2}} = p_{\mathrm{F}}^{2} \left(\frac{\partial \phi}{\partial X} \right) e^{\phi} \left\{ \left(\frac{\partial \phi}{\partial X} \right) (2p_{\mathrm{F}} e^{\phi} - 1) \left[\frac{\hbar \omega}{2} N(N - 1) - \nu \right] - 2 \left(\frac{\partial U_{\mathrm{F}}}{\partial X} - \frac{\partial U_{\mathrm{B}}}{\partial X} - \frac{\partial \nu}{\partial X} \right) \right\} + p_{\mathrm{F}} \left(\frac{\partial^{2} U_{\mathrm{F}}}{\partial X^{2}} - \frac{\partial^{2} U_{\mathrm{B}}}{\partial X^{2}} \right) + \frac{\partial^{2} U_{\mathrm{B}}}{\partial X^{2}}.$$
(C14)

Noting that the following relations for the second derivative of the bosonic and fermionic internal energies hold

$$\frac{\partial^2 U_{\rm F}}{\partial X^2} = \frac{\partial^2 U_{\rm B}}{\partial X^2}; \lim_{N \to \infty} \frac{1}{N^2} \frac{\partial^2 U_{\rm B}}{\partial X^2} = 0, \tag{C15}$$

and using Eq. (C11), the second derivatives of the internal energy read explicitly

$$\frac{1}{N^2}\frac{\partial^2 U}{\partial T^2} = \frac{\varepsilon k_{\rm B}}{8T}\frac{\left[h(d,N)+\varepsilon\right]^3}{N^2} + \frac{1}{N^2}\frac{\partial^2 U_{\rm B}}{\partial \beta^2},$$

$$\frac{1}{N^2} \frac{\partial^2 U}{\partial \nu^2} = \frac{\varepsilon \beta}{8} \left[\frac{h(d, N) + \varepsilon}{N^2} \right] - \frac{\beta}{2N^2}, \tag{C16}$$

$$\begin{split} \frac{1}{N^2} \frac{\partial^2 U}{\partial \omega^2} &= \frac{\varepsilon \hbar}{16} \frac{N(N-1)}{N^2} \left[h(d,N) + \varepsilon \right] \\ &- \frac{\hbar^2 \beta}{8} (N-1)^2 + \frac{1}{N^2} \frac{\partial^2 U_{\rm B}}{\partial \beta^2}. \end{split}$$

In the asymptotic limit, the derivatives in Eq. (C16) result in

$$\lim_{N \to \infty} \frac{1}{N^2} \frac{\partial^2 U}{\partial T^2} = \lim_{N \to \infty} \frac{\varepsilon k_{\rm B}}{8T} N = \infty,$$

$$\lim_{N \to \infty} \frac{1}{N^2} \frac{\partial^2 U}{\partial \nu^2} = 0, \tag{C17}$$

$$\lim_{N \to \infty} \frac{1}{N^2} \frac{\partial^2 U}{\partial \omega^2} = \lim_{N \to \infty} -\frac{\hbar^2 \beta}{8} N^2 = -\infty,$$

exhibiting phase transitions both with respect to temperature and frequency.

Appendix D: Further aspects of the quantum Stirling engine

In this appendix, we back up a few claims relating to the fermionizing/bosonizing Stirling cycle.

1. Conditions for positive work extraction

We here examine conditions under which the Stirling cycle extracts positive work. Our argument centers around derivatives of the free energy $F = -\frac{1}{\beta} \ln Z$. Considering first the derivative with respect to ν , we have

$$\begin{split} \frac{\partial F}{\partial \nu} &= -\frac{\partial}{\partial \nu} \frac{1}{\beta} \ln Z = -\frac{1}{\beta} \frac{\partial}{\partial \nu} \ln \left[\frac{\binom{d+N-1}{N} Z_{\rm F}}{p_{\rm F}} \right] \\ &= \frac{1}{\beta} \frac{\partial}{\partial \nu} \ln p_{\rm F} = \frac{1}{\beta} \frac{1}{p_{\rm F}} \frac{\partial p_{\rm F}}{\partial \nu}. \end{split} \tag{D1}$$

In the second line, we use that $Z=\frac{\binom{d+N-1}{N}Z_{\rm F}}{p_{\rm F}}$, which follows from the definition of $p_{\rm F}$ in Eq. (19). In the third, we used the fact that $\binom{d+N-1}{N}Z_{\rm F}$ does not depend on ν . We now note that, from Eq. (C3) for $X=\nu$

$$\frac{\partial p_{\rm F}}{\partial \nu} = \frac{\partial}{\partial \nu} \left\{ 1 + \exp\left[\frac{1}{2}N(N-1)\beta\hbar\omega - \beta\nu - h(d,N)\right] \right\}^{-1}$$

$$= p_{\rm F}^2 \beta \exp\left[\frac{1}{2}N(N-1)\beta\hbar\omega - \beta\nu - h(d,N)\right], \tag{D2}$$

and therefore

$$\frac{\partial F}{\partial \nu} = p_{\rm F} \exp \left[\frac{1}{2} N(N-1) \beta \hbar \omega - \beta \nu - h(d, N) \right], \quad (D3)$$

which is non-negative. Physically, $-\frac{\partial F}{\partial \nu}$ represents the rate at which work is done by the system when raising ν . We can therefore infer that raising ν always costs work, while lowering ν results in work extraction. However, the sign of the net work output of the whole cycle is still not clear. We consider the derivative $\frac{\partial^2 F}{\partial \beta \partial \nu}$

$$\begin{split} \frac{\partial^2 F}{\partial \beta \partial \nu} &= p_{\rm F} \frac{\partial}{\partial \beta} \exp \left[\frac{1}{2} N(N-1) \beta \hbar \omega - \beta \nu - h(d,N) \right] \\ &+ \exp \left[\frac{1}{2} N(N-1) \beta \hbar \omega - \beta \nu - h(d,N) \right] \frac{\partial p_{\rm F}}{\partial \beta} \\ &= \exp \left[\frac{1}{2} N(N-1) \beta \hbar \omega - \beta \nu - h(d,N) \right] \\ &\left\{ \left[\frac{1}{2} N(N-1) \hbar \omega - \nu \right] p_{\rm F} + \frac{\partial p_{\rm F}}{\partial \beta} \right\}. \end{split} \tag{D4}$$

Here, the derivative of $p_{\rm F}$ with respect to β , from Eq. (C3) for $X = \beta$, reads

$$\frac{\partial p_{\rm F}}{\partial \beta} = \frac{\partial}{\partial \beta} \left\{ 1 + \exp\left[\frac{1}{2}N(N-1)\beta\hbar\omega - \beta\nu - h(d,N)\right] \right\}^{-1}$$

$$= -p_{\rm F}^2 \frac{\partial}{\partial \beta} \exp\left[\frac{1}{2}N(N-1)\beta\hbar\omega - \beta\nu - h(d,N)\right]$$

$$= -p_{\rm F}^2 \left[\frac{1}{2}N(N-1)\hbar\omega - \nu\right]$$

$$\exp\left[\frac{1}{2}N(N-1)\beta\hbar\omega - \beta\nu - h(d,N)\right],$$
(D5)

so that

$$\frac{\partial^2 F}{\partial \beta \partial \nu} = \exp\left[\frac{1}{2}N(N-1)\beta\hbar\omega - \beta\nu - h(d,N)\right]$$

$$\left[\frac{1}{2}N(N-1)\hbar\omega - \nu\right] \left(p_{\rm F} - p_{\rm F}^2\right).$$
(D6)

In this expression, the exponential factor as well as $(p_{\rm F}-p_{\rm F}^2)$ are guaranteed to be non-negative, since $0 \le p_{\rm F} \le 1$. Therefore, $\frac{\partial^2 F}{\partial \beta \partial \nu}$ takes the same sign as the remaining factor $\frac{1}{2}N(N-1)\hbar\omega - \nu$. In particular, this means that if $\nu < \frac{1}{2}N(N-1)\hbar\omega$, then $\frac{\partial^2 F}{\partial \beta \partial \nu} \ge 0$ and the work cost $\frac{\partial F}{\partial \nu}\delta\nu$ of raising through a small increment $\delta\nu$ is monotone-increasing with β . It follows that if $\beta_{\rm H} > \beta_{\rm C}$ and $\nu_2 < \nu_1 < \frac{1}{2}N(N-1)\hbar\omega$, then the work cost of raising from ν_2 to ν_1 at $\beta_{\rm C}$ (i.e. fermionizing at low temperature) is less than the work extraction when lowering from ν_1 to ν_2 at $\beta_{\rm H}$ (bosonizing at high temperature). The net result is positive work extraction.

A reversal takes place if $\nu_2 > \nu_1 > \frac{1}{2}N(N-1)\hbar\omega$: the magnitude of work is monotone-increasing with β (decreasing with temperature) due to the change of sign of $\frac{\partial^2 F}{\partial \beta \partial \nu}$. In that case, positive net work extraction is achieved when bosonization (work extraction) takes place at the colder temperature, and fermionization happens at the hotter.

If ν crosses the threshold value $\frac{1}{2}N(N-1)\hbar\omega$ during the cycle, then the sign of $\frac{\partial^2 F}{\partial \beta \partial \nu}$ is not constant, and the above reasoning cannot be used to determine the sign of work extraction.

2. Recovering Carnot efficiency

We here consider the efficiency of the Carnot cycle in the limit as $\nu_1 \to -\infty$ and $\nu_2 \to +\infty$. Taking an informal approach, from Eq. (19) it can be seen that $\lim_{\nu_2 \to +\infty} p_{\rm F}(\beta, \nu_2) = 1$ Considering the total work for the cycle from Eq. (29) as $\nu_2 \to +\infty$, we have the following limit for $W^{\rm cyc}$

$$W^{\text{cyc}} \to \frac{1}{\beta_{\text{H}}} \ln \left[\frac{p_{\text{F}}(\beta_{\text{H}}, \nu_{1})}{1} \right] + \frac{1}{\beta_{\text{C}}} \ln \left[\frac{1}{p_{\text{F}}(\beta_{\text{C}}, \nu_{1})} \right]. \tag{D7}$$

On the other hand, as $\nu_1 \to -\infty$,

so that

$$p_{\rm F}(\beta, \nu_1) \to \frac{1}{\exp\left[\frac{1}{2}N(N-1)\beta\hbar\omega - \beta\nu_1 - h(d, N)\right]},$$
 (D8)

$$W^{\text{cyc}} \to -\frac{1}{\beta_{\text{H}}} \ln \left\{ \exp \left[\frac{1}{2} N(N-1)\beta_{\text{H}} \hbar \omega - \beta_{\text{H}} \nu_{1} - h(d, N) \right] \right\} + \frac{1}{\beta_{\text{C}}} \ln \left\{ \exp \left[\frac{1}{2} N(N-1)\beta_{\text{C}} \hbar \omega - \beta_{\text{C}} \nu_{1} - h(d, N) \right] \right\}$$

$$= -\left[\frac{1}{2} N(N-1) \hbar \omega - \nu_{1} - \frac{1}{\beta_{\text{H}}} h(d, N) \right] + \left[\frac{1}{2} N(N-1) \hbar \omega - \nu_{1} - \frac{1}{\beta_{\text{C}}} h(d, N) \right]$$

$$= \left(\frac{1}{\beta_{\text{H}}} - \frac{1}{\beta_{\text{C}}} \right) h(d, N). \tag{D9}$$

This gives us the first line of Eq. (31). To find the limit of Eq. (30), first note that we have already seen that

$$\begin{split} \frac{1}{\beta_{\mathrm{H}}} \ln \left[\frac{p_{\mathrm{F}}(\beta_{\mathrm{H}}, \nu_{1})}{p_{\mathrm{F}}(\beta_{\mathrm{H}}, \nu_{2})} \right] \rightarrow \\ - \left[\frac{1}{2} N(N-1) \hbar \omega - \nu_{1} - \frac{1}{\beta_{\mathrm{H}}} h(d, N) \right]. \end{split} \tag{D10}$$

It remains to find an expression for the difference in internal energy. Since $p_{\rm F}(\beta,\nu_2) \to 1$ and $p_{\rm F}(\beta,\nu_1) \to 0$,

then using Eq. (20) followed by Eq. (21), we can write

$$U(\beta_{\rm H}, \nu_2) - U(\beta_{\rm C}, \nu_1) \to U_{\rm F}(\beta_{\rm H}) - [\nu_1 + U_{\rm B}(\beta_C)]$$

$$= \frac{1}{2}N(N-1)\hbar\omega - \nu_1 + \sum_{k=1}^{N} \frac{k\hbar\omega}{e^{k\beta_{\rm H}\hbar\omega} - 1} - \frac{k\hbar\omega}{e^{k\beta_{\rm C}\hbar\omega} - 1}.$$
(D11)

Combining Eqs. (D10) and (D11), according to Eq. (30), the heat absorbed is simply

$$Q_{\rm H} \to \frac{1}{\beta_{\rm H}} h(d,N) + \sum_{k=1}^{N} \left(\frac{k\hbar\omega}{e^{k\beta_{\rm H}\hbar\omega} - 1} - \frac{k\hbar\omega}{e^{k\beta_{\rm C}\hbar\omega} - 1} \right). \tag{D12}$$